



Ricerca di Sistema elettrico

Results of the validation campaign of neutronic codes and recommendations for the correct application to LFR systems

M. Sarotto, G. Grasso

RESULTS OF THE VALIDATION CAMPAIGN OF NEUTRONIC CODES AND RECOMMANDATIONS FOR THE CORRECT APPLICATION TO LFR SYSTEMS

M. Sarotto (ENEA), G. Grasso (ENEA)

Settembre 2016

Report Ricerca di Sistema Elettrico

Accordo di Programma Ministero dello Sviluppo Economico - ENEA

Piano Annuale di Realizzazione 2015

Area: Generazione di Energia Elettrica con Basse Emissioni di Carbonio

Progetto: Sviluppo competenze scientifiche nel campo della sicurezza nucleare e collaborazione ai programmi internazionali per il nucleare di IV Generazione.

Linea: Collaborazione ai programmi internazionali per il nucleare di IV Generazione

Obiettivo: Progettazione di sistema e analisi di sicurezza

Responsabile del Progetto: Mariano Tarantino, ENEA

Titolo

RESULTS OF THE VALIDATION CAMPAIGN OF NEUTRONIC CODES AND RECCOMANDATIONS FOR THE CORRECT APPLICATION TO LFR SYSTEMS

Descrittori
Tipologia del documento: Rapporto Tecnico

Collocazione contrattuale: Accordo di programma ENEA-MSE su sicurezza nucleare e reattori di IV generazione

Argomenti trattati: Reattori nucleari veloci, Neutronica

Sommario

Questo documento riassume il lavoro svolto per il terzo obiettivo della task A.1 della Linea Progettuale 2 dell'Accordo di Programma tra ENEA e MiSE (AdP PAR2015 LP2 A.1_c). Nella progettazione di nocciolo di un reattore nucleare è fondamentale la validazione degli strumenti di analisi utilizzati per la caratterizzazione delle configurazioni oggetto di studio. Facendo riferimento ai sistemi veloci refrigerati a piombo, è al momento scarsa l'attività di validazione delle metodologie e dei codici di analisi neutronica, mentre svariate attività sono state svolte in passato per gli strumenti di analisi termoidraulica. Per questo motivo è stata pianificata un'attività estensiva di validazione che si articola sui tre anni dell'AdP, avvalendosi dei risultati delle prove sperimentali effettuate in due reattori nucleari di ricerca a potenza zero:

- VENUS-F, presso il centro ricerche SCK•CEN (Belgio);
- LR-0, presso il centro ricerche CV-Řež (Repubblica Ceca).

In questa prima annualità sono state effettuate attività su entrambi i fronti, e specificamente:

- è stata progettata e realizzata una sezione di prova per il reattore LR-0 e sono stati messi a punto i modelli di calcolo stocastici per la riproduzione dei risultati delle prove sperimentali previste in tale reattore;
- sono state riprodotte alcune condizioni realizzate sperimentalmente nel reattore VENUS-F, durante il progetto EURATOM FP7 FREYA in una configurazione di nocciolo rappresentativa del LFR, e sono stati interpretati alcuni risultati ottenuti con tali prove.

Lo strumento impiegato per l'analisi delle prove sperimentali nel reattore VENUS-F è il codice neutronico deterministico ERANOS, per mezzo del quale:

- è stata svolta un'analisi di sensibilità ed incertezza per il fattore di moltiplicazione efficace, in aggiunta ad uno studio preliminare di alcuni coefficienti di reattività e dei principali parametri cinetici;
- è stata eseguita una valutazione del rapporto calcolo-esperimento per alcuni indici di spettro e per l'anti-reattività inserita dalla barra di controllo di maggiore interesse.

Note
Autori: M. Sarotto¹, G. Grasso¹
¹ ENEA

Copia n.
In carico a:

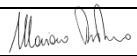
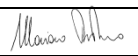

| | | | | | | |
|------|-------------|----------|-----------|--|---|---|
| 2 | | | NOME | | | |
| | | | FIRMA | | | |
| 1 | | | NOME | | | |
| | | | FIRMA | | | |
| 0 | EMISSIONE | 20/09/16 | NOME | M. Sarotto | M. Tarantino | M. Tarantino |
| | | | FIRMA |  |  |  |
| REV. | DESCRIZIONE | DATA | REDAZIONE | CONVALIDA | APPROVAZIONE | |

TABLE OF CONTENTS

| | |
|--|----|
| Acronyms and Abbreviations..... | 3 |
| 1. Introduction..... | 4 |
| 2. Simulation tools considered for their validation..... | 6 |
| 2.1. The ERANOS deterministic code..... | 6 |
| 2.2. The MCNP Monte Carlo code..... | 6 |
| 3. The VENUS-F core design for LFR experiments..... | 7 |
| 3.1. Rationale..... | 7 |
| 3.2. The VENUS-F core design representative of the LFR spectrum | 8 |
| 4. The ERANOS code validation with VENUS-F experiments | 10 |
| 4.1. Control Rod worth..... | 10 |
| 4.2. The spectrum indexes | 11 |
| 4.3. Impact on k_{eff} value of some materials properties | 12 |
| 4.4. Impact of neutron library on kinetic parameters | 14 |
| 5. The LR-0 experiments in support of the LFR..... | 15 |
| 6. Concluding discussion and successive steps..... | 18 |
| References | 20 |
| Appendix A - Sensitivity and uncertainty analyses on k_{eff} value..... | 22 |
| A.1. Brief summary of background theory..... | 22 |
| A.2. Results and discussion | 24 |

Acronyms and Abbreviations

| | |
|------------------|---|
| AIA | Alfred Inert Assembly(ies) |
| ALFRED | Advanced Lead-cooled Fast Reactor European Demonstrator |
| C/E | Calculated-to-Experimental |
| CR | Control Rod(s) |
| EFA | Experimental Fuel Assembly(ies) |
| ERANOS | European Reactor ANalysis Optimised System |
| FA | Fuel Assembly(ies) |
| FREYA | Fast Reactor Experiments for hYbrid Applications |
| F25 | Fission rates of ${}_{92}\text{U}^{235}$. Similarly: F28 = Fission ${}_{92}\text{U}^{238}$, F37 = Fission ${}_{93}\text{Np}^{237}$ F49 = Fission ${}_{94}\text{Pu}^{239}$, F41 = Fission ${}_{94}\text{Pu}^{241}$, C28 = Capture ${}_{92}\text{U}^{238}$ |
| LA | Lead Assembly(ies) |
| LEADER | Lead-cooled European Advanced DEmonstration Reactor |
| FP | Framework Program |
| GIF | Generation IV International Forum |
| k_{eff} | Effective multiplication factor |
| LFR | Lead Fast Reactor(s) |
| MCNP | Monte Carlo Neutron Particle |
| MOX | Mixed OXide |
| pcm | per cent mille |
| SR | Safety Rod(s) |
| SS | Stainless Steel |
| VENUS-F | Vulcan Experimental NUclear Study-Fast |
| WP | Work Package |

| | | | | | |
|--|---------------------------------|-------------|-----------------|-------------|-----------|
|  Ricerca Sistema Elettrico | Sigla di identificazione | Rev. | Distrib. | Pag. | di |
| | ADPFISS – LP2 – 115 | 0 | L | 4 | 32 |

1. Introduction

This work is inserted in the framework of the Programmatic Agreement (Accordo di Programma, AdP PAR 2015) between ENEA and MiSE (Ministero dello Sviluppo Economico): it deals with the validation of the neutronic codes used for the core design of Lead Fast Reactors (LFR). This activity is fundamental to obtain the level of confidence in the results, that is required to size the precision by which the target limits are met or not. The relevancy of this work is even more emphasized by the consideration that, whilst validation activities related to thermal-hydraulic analyses were widely carried out in the past, a similar effort related to the methodologies and tools for the neutronic analyses has not yet been done.

The LFR chosen as reference is represented by the Advanced Lead Fast Reactor European Demonstrator (ALFRED), whose design was initially conceived in the Lead-cooled European Advanced DEMonstration Reactor (LEADER) project of the 7th EURATOM Framework Program (FP7) [1]. By adopting as leading criteria the ambitious concepts expressed by the Generation IV International Forum (GIF), the LFR could represent a promising technology for a new generation of nuclear energy systems more safe, clean, economical and proliferation resistant [2].

When considering the validation of simulation tools and design procedures of a new reactor concept, several phenomena have to be addressed and their effects assessed. Focusing on the effects, two categories can be pointed out, to each of which also correspond some generic conditions to be achieved in research reactors for letting these effects emerge:

- fixed effects caused by the phenomena intervening in changing the elementary properties of the system, and
- effects progressively increasing as a function of the accumulated consequences of the phenomena these are caused by.


The phenomena whose effects belong to the second group typically need high flux reactors, so that the accumulation of the consequences can achieve measurable effects in a reasonable amount of time. Due to the current availability of zero-power reactors only, this study will be focused to the phenomena belonging to the first group.

The envisaged campaign of neutronic modelling and analyses of experiences representative of the LFR begins, with the present study, by taking as reference two zero-power reactors:

- the Vulcan Experimental Nuclear Study-Fast (VENUS-F) facility, located at the SCK•CEN research centre in Mol, Belgium [3];
- the LR-0 reactor, located at the CVR research centre in Řež, Czech Republic [4].

In VENUS-F, some experiments representative of the ALFRED LFR concept were performed within the scope of the Work Package 4 (WP4) of the EURATOM FP7 Fast Reactor Experiments for hYbrid Applications (FREYA) project [5-8]. The validation activity was focused on the ERANOS deterministic code [9-11], whose main features are summarised in §2, coupled with the JEFF3.1 [12] and the ENDF/B-VI.8 [13] data libraries. The VENUS-F critical core layout representative of the LFR (called “CC6” core) is briefly described in §3.

In this report, some fundamental physical quantities for the core design - that were not analysed in details during the FREYA project [7-8] - were considered:

| | | | | | |
|--|---------------------------------|-------------|-----------------|-------------|-----------|
|  Ricerca Sistema Elettrico | Sigla di identificazione | Rev. | Distrib. | Pag. | di |
| | ADPFISS – LP2 – 115 | 0 | L | 5 | 32 |


- the spectrum indexes and the anti-reactivity inserted by a single Control Rod (CR), through the evaluation of the Calculated-to-Experimental ratio (C/E) (see §4.1-4.2);
- the effective multiplication factor k_{eff} , by investigating the impact on its value due to small variations of the properties of the main materials in the fissile zone (see §4.3);
- the kinetic parameters, by investigating the influence of the nuclear data library chosen on their values (see §4.4).

Furthermore, for what concerns the effective multiplication factor, Appendix A reports quite detailed sensitivity and uncertainty analyses performed in order to evaluate the impact of the neutron cross-section uncertainties on the k_{eff} value.

About the activities related to the LR-0 reactor, its extreme flexibility allows the arrangement of dry test sections, decoupled from the multiplying region sustaining the chain reaction, where flux adjustments can be performed to allow experiments on neutrons propagation and power distribution. In particular, and thanks to the extremely precise measurement devices available in the laboratories connected with the reactor, the following investigations can be envisaged:

- local evaluation of the power distribution in a multiplying medium in a LFR representative spectrum;
- local evaluation of the captures distribution in a medium in a LFR representative spectrum.

As briefly described in §5, within the scope of the first year of the present tri-annual program of the AdP, the design and preliminary characterization of an experimental test section allowing the above mentioned investigations has been performed. Due to the local extent of the measurements envisaged in the test section, the stochastic MCNP code (presented in §2) was chosen as reference.

| | | | | | |
|--|---------------------------------|-------------|-----------------|-------------|-----------|
|  Ricerca Sistema Elettrico | Sigla di identificazione | Rev. | Distrib. | Pag. | di |
| | ADPFISS – LP2 – 115 | 0 | L | 6 | 32 |

2. Simulation tools considered for their validation

2.1. *The ERANOS deterministic code*

Large part of the neutronic analyses - finalised to its validation for the LFR core design - was carried out with the European Reactor ANalysis Optimised System (ERANOS) version 2.2 deterministic code [9]. It is a modular system with different modules that perform several functions to analyse reactivity, fluxes, burn-up, reaction rates, etc. of a nuclear system that can be modelled by 1D, 2D and 3D geometries. The macroscopic cross-sections of the different zones of the core (*e.g.*, fissile zone, axial and radial reflectors) are obtained by means of the European Cell Code (ECCO) [10]. In this work, an accurate 2D geometry description of such zones in the VENUS-F facility (described in §3) was adopted, while the axial leakages were taken into account by tuning opportunely the bucking value [10].

The full core calculations were carried out with the TGV module [11], in which a 3D geometrical description of the whole reactor was implemented. For what concerns the activities related to the simulation of the experiments carried out during the EURATOM FP7 FREYA project (§3-4):

- the TGV module exploits the variational nodal method [11] to solve the transport equation in a 3D XYZ geometry model of the core;
- the analyses were performed by adopting the JEFF3.1 [12] and ENDF/B-VI.8 [13] nuclear data libraries available in the ECCO/ERANOS environment;
- the macroscopic cross-sections of the different core / reactor regions were produced in ECCO by a 1968 energy-group structure and then condensed in an “optimised” energy structure at 49 groups [14]. Otherwise, the sensitivity analyses reported in Appendix A were carried out by condensing the results in the standard energy structure at 33 groups [10], as well as the evaluation of the kinetic parameters (§4.4). The uncertainty analyses (reported also in Appendix A) were performed by adopting 15 energy groups, because of the covariance matrix adopted [15].

2.2. *The MCNP Monte Carlo code*

For what concerns the activities related to the LR-0 reactor (§5), due to the local nature of the phenomena being investigated, the Monte Carlo Neutron Particle (MCNP) code ver. 6.1 [16] was assumed as reference, coupled with the ENDF/B-VII.0 nuclear data library [17]. Stochastic codes, indeed, have the capability to better reproduce local phenomena – provided that a sufficient statistic is ensured by tuning the parameters of the simulations, whose optimization is part of the validation process itself (object of the study) – thanks to the exact heterogeneous description of the model geometry and the continuous treatment of the energy dependence of neutron-matter interactions.

3. The VENUS-F core design for LFR experiments

3.1. Rationale

When addressing the core design (and in perspective the licensing) of a new reactor concept as the LFR, a thorough validation of neutronic calculation codes (and data libraries) is deemed necessary to prove, to the largest extent, the validity of the results and the appropriateness of the design methodologies and tools. The VENUS-F reactor in the FREYA EU FP7 project represented an opportunity to perform integral tests and local measurements of neutronic parameters representative of the LFR, in order to support the validation of both deterministic and Monte Carlo neutron transport codes. As pointed out in [6], the most aimed requirement for this validation process is the achievement of a “LFR representative spectrum” for the main neutronic parameters under study.

The LFR design chosen as reference is ALFRED, whose design was initially conceived during the LEADER EU FP7 project (§1). As described in [1], the core is made of hexagonal and wrapped Fuel Assemblies (FAs) with 127 Mixed OXide (MOX) fuel pins in a triangular lattice. For power distribution flattening, the core is divided in two radial zones - inner and outer - having ≈ 22 and ≈ 28 wt.% Plutonium enrichment, respectively.

Figure 3.1 shows the typical “clean” VENUS-F critical layout defined in the FREYA activities named “CC5 core” [5]. Besides the FA (purple) having a ≈ 600 mm fissile length, the layout is essentially made of six fuel follower Safety Rods (SR1-6), two CR (CR1-2) and the surrounding Lead Assemblies (LA, light blue). The absorbing parts of both the SRs and CRs are made of boron carbide (B_4C), as in the ALFRED LFR design.

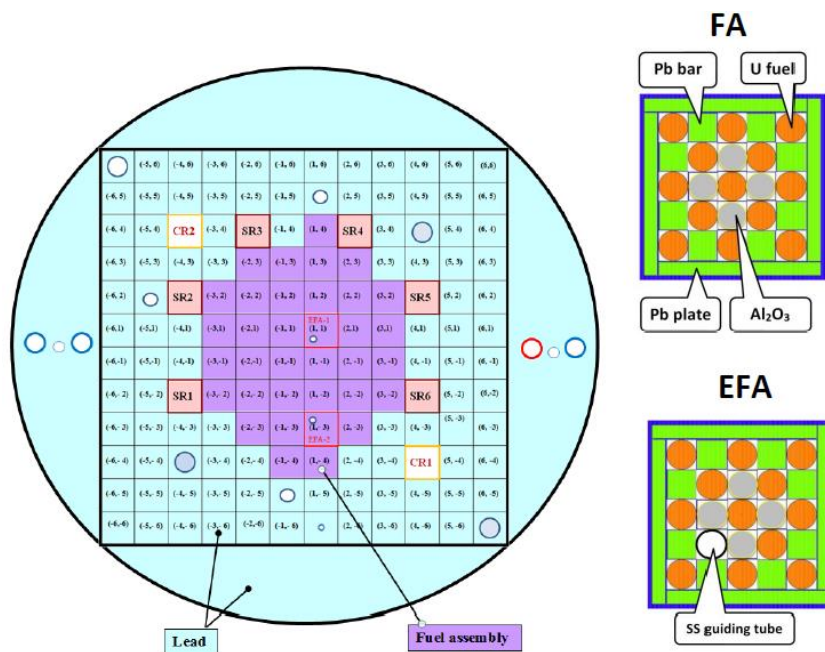


Figure 3.1 The “clean” CC5 VENUS-F critical core layout [5].

As depicted in the right part of Figure 3.1, the FA is arranged in a 5x5 square matrix made of:

- 13 fuel pins containing metallic Uranium enriched at 30 wt.% in U^{235} ;

- 8 Pb bars to simulate the lead coolant;
- 4 Al₂O₃ rodlets to soften the hard neutron flux of metallic fuel so as to simulate the MOX fuel actually foreseen for ALFRED;
- a surrounding Pb plate enclosed in a Stainless Steel (SS) box.

Furthermore, as also shown in Figure 3.1, two Experimental FAs (EFA-1 and EFA-2) were foreseen for axial traverse measurements into the fissile zone, in which a fuel rod in the FA was replaced by an empty SS guiding tube in which the detectors were inserted.

Despite the presence of the Al₂O₃ rodlets, the VENUS-F FA spectrum resulted to be significantly harder than the ALFRED one (*i.e.*, LFR with MOX fuel). This difference of spectra is clearly shown in the ERANOS results of Figure 3.2 wherein, since ALFRED is a fast reactor, the analysis is focused on the fast part of the spectrum above 1 keV¹. By adopting a 49 energy-group-structure [14], the normalised flux per unit lethargy is represented for the CC5 core (of Figure 3.1, in the EFA-2 position at core mid-plane), the ALFRED inner and outer FA [1].

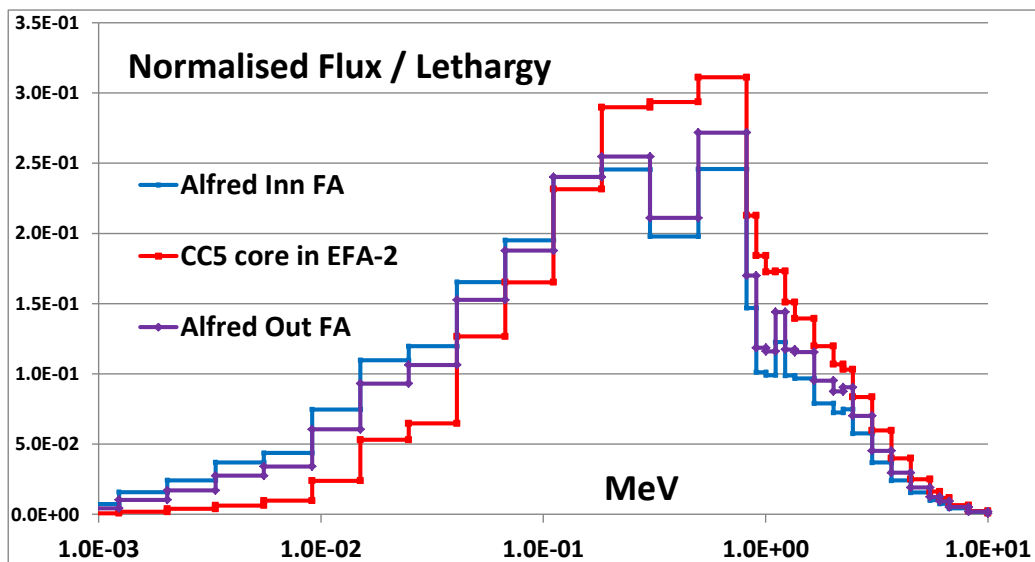


Figure 3.2 Comparison between the CC5 core, ALFRED inner and outer FA spectra evaluated with ERANOS in the [1E-3, 10] MeV range (semi-logarithmic scale).

3.2. The VENUS-F core design representative of the LFR spectrum

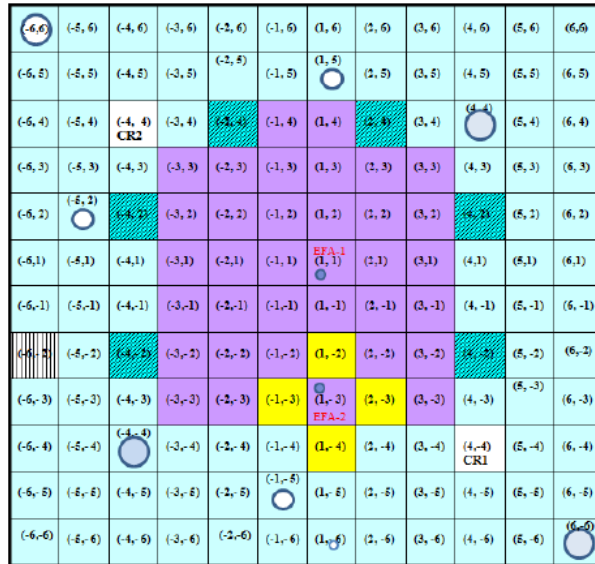
To simulate the ALFRED (LFR-MOX) spectrum, some moderating assemblies – made only by Al₂O₃ rodlets (# 25) and called Alfred Inert Assembly (AIA) – were inserted in the VENUS-F core layout. A combination of 3x3 assemblies - called “ALFRED island” and made by FA, AIA and LA disposed as a chess - was foreseen around the EFA-2 position in order to reproduce in it the wished spectrum [6]. Figure 3.3 depicts the resulting critical core layout named “CC6 core” in FREYA [5], while Figure 3.4 compares:

- the aimed ALFRED (inner and outer FA) spectra evaluated with ERANOS;

¹ The lower energy limit used for fast spectra analyses depends on the application (*e.g.*, materials damage, actinides transmutation performances, etc.) and usually ranges from 0.1 to 1 MeV: 1 keV is therefore a conservative threshold.

- the spectra obtained in the CC6 core in EFA-2 position at core mid-plane, evaluated with ERANOS and the Monte Carlo code MCNP ver. 6 [6].

It can be noticed the optimal agreement between deterministic and Monte Carlo results and, mostly, to which extent the spectrum obtained in EFA-2 position reproduces properly the aimed ALFRED ones.



| | Amount |
|--|--------|
| - lead assemblies, PbA, Pb50, Pb31, Pb10 | 96 |
| - FA – fuel assembly | 35 |
| - control rods "CR" | 2 |
| - rod drop | 1 |
| - safety rods, SR | 6 |
| - Alfred Inert Assembly (AIA) | 4 |

Figure 3.3 The VENUS-F CC6 critical core representative of the LFR spectrum [5].

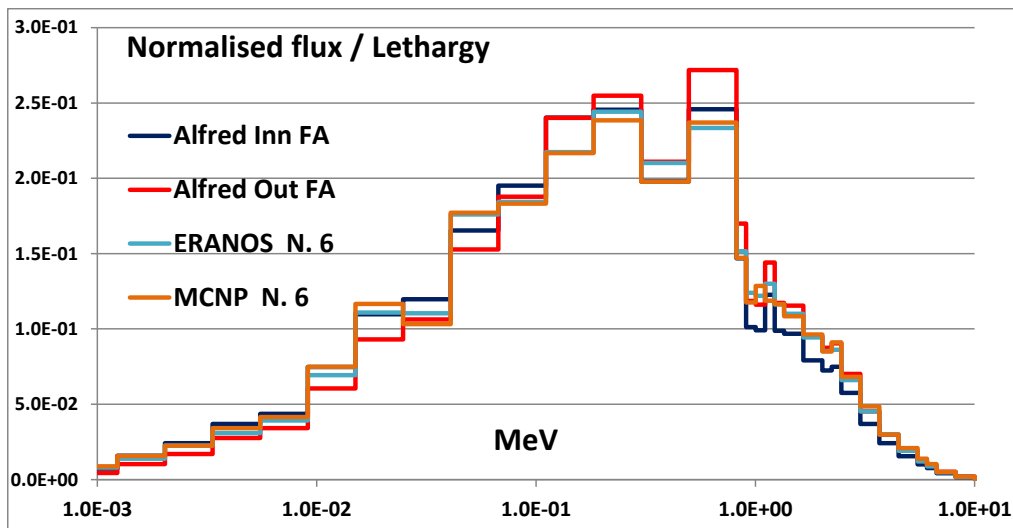



Figure 3.4 ERANOS and MCNP6 spectra in EFA-2 position in the CC6 core compared with the ALFRED ones in the [1E-3, 10] MeV range (semi-logarithmic scale).

| | | | | | |
|--|---------------------------------|-------------|-----------------|-------------|-----------|
|  Ricerca Sistema Elettrico | Sigla di identificazione | Rev. | Distrib. | Pag. | di |
| | ADPFISS – LP2 – 115 | 0 | L | 10 | 32 |

4. The ERANOS code validation with VENUS-F experiments

Starting from the critical mock-up representative of the ALFRED LFR defined and assembled in the VENUS-F zero-power reactor (named CC6 core, Figure 3.3), detailed characterisation measurements were performed during the FREYA project: the main results are reported in [7]. Successively, the C/E comparisons between neutronic codes and the characterisation measurements were performed and reported in [8]. A general and good C/E agreement was found for both standard and void effect measurements, but some aspects need to be further investigated. Therefore, the validation activity concerning the ERANOS deterministic code is integrated in this report that results to be complementary with [8].

As mentioned in §1, some fundamental physical quantities for the core design are here investigated:

- the anti-reactivity inserted by the single CR close to the ALFRED island (CR1 in Figure 3.3), whereas the C/E results reported in [8] concern both CRs (see §4.1);
- the spectrum indexes in the EFA-2 position, since some C/E values obtained in [5, 8] resulted to be not satisfactory (see §4.2);
- the impact on the k_{eff} value due to the variation of the density of the materials composing the fissile zone, the fuel enrichment and its temperature (see §4.3);
- the influence of the nuclear data library on the kinetic parameters, as the effective delayed neutron fraction (β_{eff}) and neutron generation lifetime (Λ_{eff}) (see §4.4).

4.1. Control Rod worth

The measurements on CR calibration and worth were carried out in FREYA with a standard FA replacing EFA-2 in the layout of Figure 3.3 [7]. Most of the measurements and related code simulations were focused on the experimental results obtained by moving both CRs together [8]. Additionally, few measurements were devoted to the calibration of each CR separately [7]. In order to validate the ERANOS results for the LFR concept, it results interesting to analyse the anti-reactivity inserted by the CR close to the ALFRED island (called CR1, see Figure 3.3).

As reported in [7], the anti-reactivity inserted by CR1 only was measured at 50 mm steps from 350 mm up to 600 mm, representing the completely withdrawn position (*i.e.*, ≈ 600 mm fissile length). By assigning at each movement step the coordinate of the middle point, Table 4.1 reports the C/E values obtained with ERANOS coupled with the JEFF3.1 and ENDF/B-VI.8 nuclear data libraries. It can be noticed that:

- the ERANOS results obtained with both libraries slightly under-estimate the actual anti-reactivity inserted in each CR1 step;
- the ERANOS-ENDF/B-VI.8 values resulted to be more accurate than the ERANOS-JEFF3.1 ones;
- the accuracy can be as low as 8% / 6% with JEFF3.1 / ENDF/B-VI.8 library, respectively, while the measurement uncertainties on the CR worth was limited to about 3%.

Table 4.1 C/E values for CR1 anti-reactivity worth at different insertion heights (Z) obtained with the ERANOS code coupled with JEFF3.1 and ENDF/B-VI.8 nuclear data.

| Z [mm] | C/E with ERANOS for CR1 worth | |
|-------------------------|--------------------------------------|--------------------|
| | JEFF3.1 | ENDF/B-VI.8 |
| 375 | 0.985 | 0.997 |
| 425 | 0.935 | 0.948 |
| 475 | 0.921 | 0.965 |
| 525 | 0.921 | 0.942 |
| 575 | 0.987 | 0.975 |

4.2. The spectrum indexes

The spectrum indexes of main interest in a fast spectrum were measured in the EFA-2 position at the CC6 core mid-plane (Figure 3.3), where the ALFRED LFR spectrum was reproduced (Figure 3.4). Three fission rate ratios were measured: F28/F25, F49/F25 and F37/F25 [7].

The spectrum index values were obtained with ERANOS (in EFA-2 position at CC6 core mid-plane) by the ratio of the following reaction rates:

$$SI^r = \frac{\sum_g \sigma_g^r \phi_g}{\sum_g \sigma_g^{F25} \phi_g} \quad (4.1)$$

where:

- SI^r is the spectrum index value for F28/F25, F49/F25 and F37/F25;
- ϕ_g is the flux value in each energy group g (1-49);
- σ_g^{F25} is the ${}_{92}\text{U}^{235}$ fission microscopic cross-section value in each energy group g (1-49);
- σ_g^r is the fission microscopic cross-section value for the nuclide of interest (*i.e.*, F28 for ${}_{92}\text{U}^{238}$, F49 for ${}_{94}\text{Pu}^{239}$ and F37 for ${}_{93}\text{Np}^{237}$ fission microscopic cross-sections) in each energy group g (1-49).

Table 4.2 reports the C/E values obtained with ERANOS coupled with JEFF3.1 and ENDF/B-VI.8 data libraries: it can be noticed that the accuracy varies in the 1 ÷ 5.5% range with both libraries.

Table 4.2 The ERANOS (JEFF3.1 and ENDF/B-VI.8) C/E values for spectrum indexes (in EFA-2 position at CC6 core mid-plane).

| Spectrum index | C/E | |
|-----------------------|----------------|--------------------|
| | JEFF3.1 | ENDF/B-VI.8 |
| F28 / F25 | 0.945 | 0.966 |
| F49 / F25 | 1.011 | 1.010 |
| F37 / F25 | 0.964 | 0.951 |

As described in [18], the calculation accuracy of spectrum indexes with ERANOS could be increased by replacing EFA-2 with a standard FA that avoids, at some extent, the channel

void homogenisation occurring in the EFA-2 ECCO cell calculations (providing the macroscopic cross-sections of the different reactor zones for ERANOS, §2). In this “virtual” layout with a FA replacing EFA-2, the three simulated spectrum indexes – with both libraries – differ from the experimental values less than the measurement uncertainty [8].

Nevertheless, from the “reference” ERANOS calculations - done with EFA-2 and summarised in Table 4.2 - it can be noticed that the worst C/E values appears for the F28/F25 and F37/F25 indexes, that deal with nuclides having a threshold fission cross-section (U^{238} and Np^{237}). As suggested in [5] and referring to the F28/F25 value, the high discrepancy could be due to the presence of U^{235} impurities in the U^{238} fission chamber deposit of about 0.36%. Actually, as shown in Figure 4.1, the C/E value improves significantly by assuming a tiny U^{235} impurity in the U^{238} chamber. But, the level of impurity that yields a C/E value closer to one for F28/F25 resulted to be $\cong 0.1\%$ / 0.2% for ENDF/B-VI.8 / JEFF3.1 data, respectively. Probably, this discrepancy (*i.e.*, $0.1 \div 0.2\%$ vs. 0.36% impurity) is due to the channel void homogenisation occurring in the EFA-2 ECCO cell calculations mentioned before.

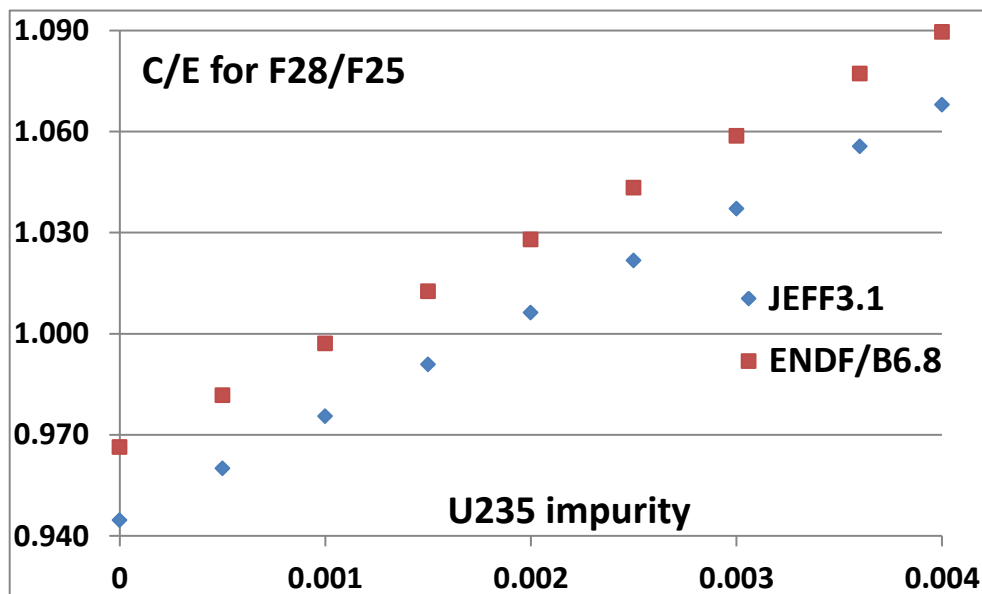


Figure 4.1 The ERANOS (JEFF3.1 and ENDF/B-VI.8) C/E values for F28/F25 spectrum index with tiny impurities of U^{235} in the U^{238} fission chamber deposit.

4.3. Impact on k_{eff} value of some materials properties

The neutronic analyses performed during FREYA pointed out a significant spread in the k_{eff} value depending on the code (Monte Carlo or deterministic) and on the library adopted [8]. Therefore, with the aim to validated the ERANOS results, it was deemed useful to study the impact on the multiplication factor of small variations in some materials properties, such as:

- the density of the materials in the fissile zone and the U^{235} enrichment in the fuel, whose results are summarised in Table 4.3;
- the temperature assumed for the fuel pins, whose results are reported in Table 4.4;
- the energy structure adopted (49 vs. 33 groups, §2), whose results are reported in Table 4.5.

From Table 4.3 it appears evident that:

- the ERANOS-JEFF3.1 and ERANOS-ENDF/B-VI.8 Δk_{eff} variations expressed in per cent mille (pcm) are almost identical;
- the 1 wt.% variation of the SS, Pb and Al_2O_3 density (in fissile zone and AIA) causes a k_{eff} variation of about 20 pcm;
- the 1 wt.% variation of the U density causes a k_{eff} variation of about 460 pcm;
- the 1 wt.% variation of the U^{235} enrichment causes a k_{eff} variation of about 470 pcm.

This latter result is quite interesting (and useful) for the code validation since all calculations were carried out with the nominal 30 wt.% fuel enrichment. But, actually, for fuel ageing and short irradiation periods the actual value of the U^{235} enrichment could be slightly lower.

Table 4.3 The ERANOS (JEFF3.1 and ENDF/B-VI.8) Δk_{eff} values due to the variation of the materials density in the fissile zone and of the U^{235} fuel enrichment.

| Parameter | Δk_{eff} [pcm] | | Δk_{eff} [pcm] / 1 wt. % | |
|--|-------------------------------|-------------|---|-------------|
| | JEFF3.1 | ENDF/B-VI.8 | JEFF3.1 | ENDF/B-VI.8 |
| Pb density -5 wt. % | -90 | -90 | -18 | -18 |
| Pb density +5 wt. % | +88 | +90 | +18 | +18 |
| SS density -5 wt. % | -96 | -93 | -19 | -19 |
| SS density +5 wt. % | +94 | +92 | +19 | +18 |
| Al_2O_3 density -5 wt. % | -110 | -105 | -22 | -21 |
| Al_2O_3 density +5 wt. % | +108 | +104 | +22 | +21 |
| U density -2 wt. % | -919 | -920 | -459 | -460 |
| U density -1 wt. % | -457 | -457 | -457 | -457 |
| U^{235} enrich. -2 wt. % | -944 | -941 | -472 | -470 |
| U^{235} enrich. -1 wt. % | -470 | -469 | -470 | -469 |

Table 4.4 reports the Δk_{eff} variation with the fuel temperature, in comparison with the nominal calculations carried out at 20 °C. This evaluation was done since the actual value of the fuel temperature should be slightly higher than 20 °C because of the VENUS-F power that, actually, during criticality was not zero. Also in this case the ERANOS-JEFF3.1 and ERANOS-ENDF/B-VI.8 results are almost identical: the Δk_{eff} value are in the order of -0.5 ÷ -0.6 pcm per 1 °C variation.

Table 4.4 The ERANOS (JEFF3.1 and ENDF/B-VI.8) Δk_{eff} values due to the variation of the fuel temperature (in comparison with the nominal case at 20 °C).

| Fuel T [°C] | Δk_{eff} [pcm] | | Δk_{eff} [pcm] / 1 °C | |
|----------------|-------------------------------|-------------|--------------------------------------|-------------|
| | JEFF3.1 | ENDF/B-VI.8 | JEFF3.1 | ENDF/B-VI.8 |
| 50 | -18 | -18 | -0.60 | -0.60 |
| 100 | -44 | -45 | -0.55 | -0.56 |
| 150 | -67 | -69 | -0.52 | -0.53 |
| 200 | -87 | -90 | -0.48 | -0.50 |

Table 4.5 reports the Δk_{eff} variation with the energy group structure adopted: as mentioned in §2, besides the “reference” evaluations at 49 energy groups the ERANOS calculations were carried out also at 33 groups [10]. With both data libraries (JEFF3.1 and ENDF/B-VI.8) the ERANOS k_{eff} values obtained differ only by about 20 pcm.

Table 4.5 Influence of the energy group structure (33 and 49 groups) on the k_{eff} values obtained with ERANOS (JEFF3.1 and ENDF/B-VI.8).


| $k_{\text{eff}} (49 \text{ eg}) - k_{\text{eff}} (33 \text{ eg}) [\text{pcm}]$ | |
|--|-------------|
| JEFF3.1 | ENDF/B-VI.8 |
| 20 | 23 |

4.4. Impact of the neutron library on kinetic parameters

An additional analysis was carried out by investigating the effect of the neutron data library (JEFF3.1 and ENDF/B-VI.8) on the values of the effective delayed neutron fraction (β_{eff}) and neutron generation lifetime (Λ_{eff}). Both kinetic parameters were evaluated for the CC6 core layout (Figure 3.3) by adopting 33 energy groups and 6 groups of delayed neutrons [9-10]. Table 4.6 reports the difference due to the library chosen in the ERANOS calculations, that is limited to 1 pcm for β_{eff} and 1 μs for Λ_{eff} . Therefore, the two data libraries yield the same results, while a difference of some hundreds pcm was found in the k_{eff} values [8].

Table 4.6 Influence of the neutron data library (JEFF3.1 and ENDF/B-VI.8) on the effective delayed neutron fraction (β_{eff}) and neutron generation lifetime (Λ_{eff}) evaluated with ERANOS.

| JEFF3.1 - ENDF/B6.8 | $\Delta\beta_{\text{eff}} [\text{pcm}]$ | $\Delta\Lambda_{\text{eff}} [\mu\text{s}]$ |
|---------------------|---|--|
| | | 1 |

| | | | | | |
|--|---------------------------------|-------------|-----------------|-------------|-----------|
|  Ricerca Sistema Elettrico | Sigla di identificazione | Rev. | Distrib. | Pag. | di |
| | ADPFISS – LP2 – 115 | 0 | L | 15 | 32 |

5. The LR-0 experiments in support of the LFR

As mentioned in §1, the aim of the experiments envisaged in the LR-0 reactor are meant to the measurement of the distributions of fissions and captures occurred in fuel pins irradiated in a LFR-representative spectrum.

To meet this objective, a duly characterization of the experimental test section is required to ensure that the neutron spectrum is properly reproduced. Then, thanks to the very accurate measurement devices available in the laboratories connected with the reactor, an investigation of the power distribution in fuel elements placed within the test section can be envisaged. A 3D map of the power generation induced in these fuel elements under representative conditions would allow indeed to validate flux reconstruction techniques, hence providing significant feedbacks for the designer to assess the confidence on the results of his simulation tools with respect to the actual conditions, hence to measure the uncertainty that is to be associated to the design for safety purposes.

Although based on neutron moderation to achieve criticality, the extreme flexibility of the LR-0 zero-power reactor might allow the arrangement of dry test sections, decoupled from the multiplying region sustaining the chain reaction, where flux adjustment can be performed to allow experiments on neutrons propagation and power distribution.

The key for the success of the envisaged experiments is therefore the proper tuning of the neutron spectrum in the test section. The starting point is the arrangement of a sustaining region allowing for a dry irradiation position in it. Exploiting the extremely flexible design of the LR-0 reactor, on the core support plate enough positions are provided to arrange a compact configuration which can achieve criticality through adjustments of the water level. In particular, six FAs arranged on a hexagonal ring represent the most compact critical configuration leaving the central position free to insert a test section, as shown in Figure 5.1.

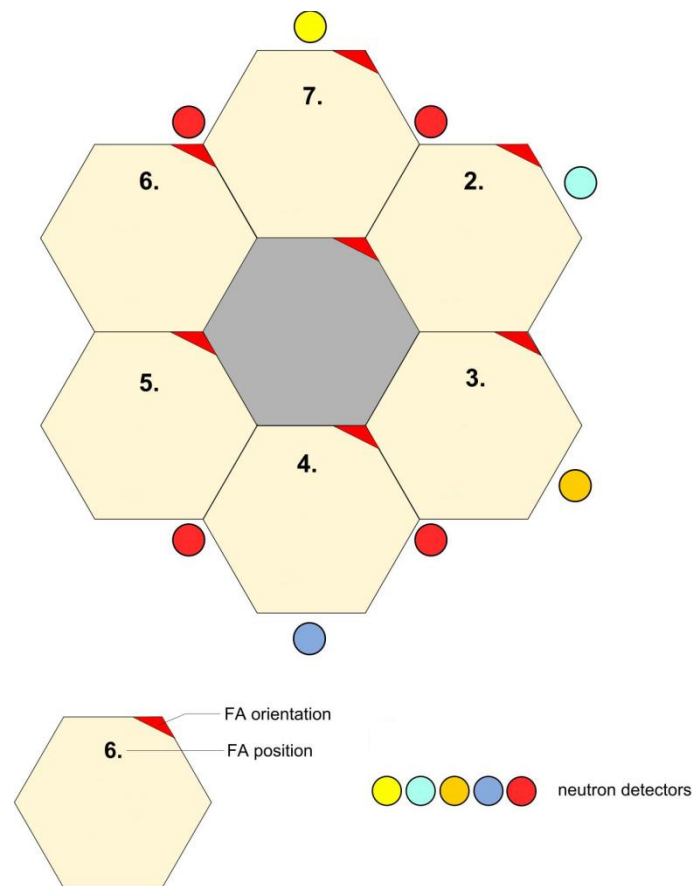


Figure 5.1 Critical configuration of the LR-0 core for the ALFRED experiments in the central test section, with positions for neutron detectors.

Figure 5.1 shows also the positions close to the core where neutron detectors can be placed for the thorough monitoring of the neutron flux and criticality, hence for the control of the experiment itself.

The test section occupying the central hexagonal position has to host the fuel elements for irradiation, as well as neutron detectors for on-site monitoring of the neutron flux. Both fuel elements and detectors placeholders are to be distributed within the test section to increase the information on the spatial distribution of the flux. Around the sensible volume for the experiments, right behind the case of the test section, neutron filters are to be envisaged to cut the thermal tail of the neutron spectrum. Then, the remaining volume has to be filled with lead to finely tune the spectrum.

The final aspect for the design of the experiment is the choice of materials and their dimensioning. To this regard, along with the neutron flux entering the central dry position as sourced by the sustaining core, it is to be considered that stilbene detectors are envisaged, whose tubes can influence not only the criticality, but also the neutron spectrum within the test section.

After extensive calculations [19] (here not reported for simplicity) an optimized configuration was identified. Figure 5.2 shows the test section realized according to the results of these studies and its relative positioning in the LR-0 core for experiments.



Figure 5.2 View of the ALFRED test section (left) and its positioning in the central hexagonal channel (right).

Finally, Figure 5.3 shows the assembling of the ALFRED configuration in the LR-0 reactor.

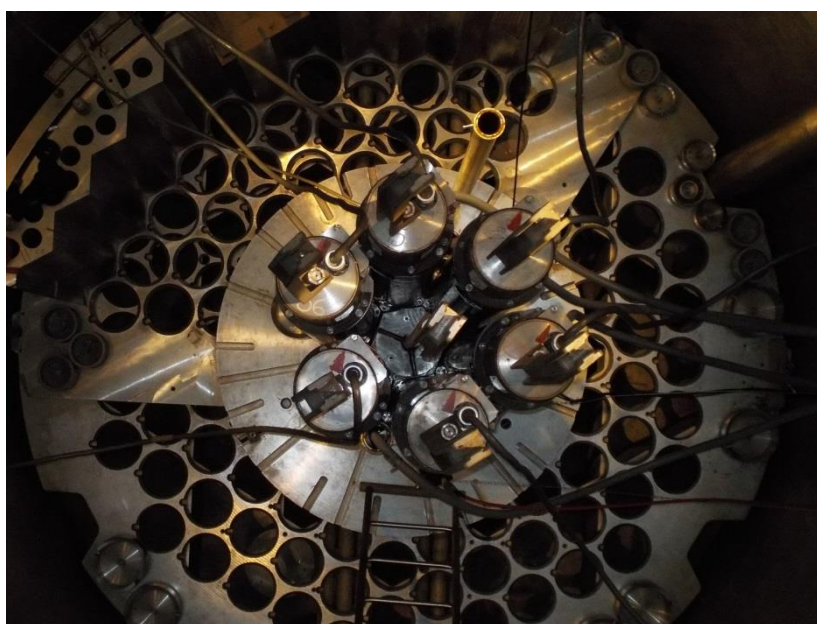



Figure 5.3 Top-view of the ALFRED configuration in the LR-0 reactor.

| | | | | | |
|--|---------------------------------|-------------|-----------------|-------------|-----------|
|  Ricerca Sistema Elettrico | Sigla di identificazione | Rev. | Distrib. | Pag. | di |
| | ADPFISS – LP2 – 115 | 0 | L | 18 | 32 |

6. Concluding discussion and successive steps

This technical report describes the achievements of the first part of the campaign performed by ENEA for the validation of neutronic codes and their correct application to LFR systems as the ALFRED reactor concept. The experimental tests carried out or planned in two zero-power reactors – VENUS-F and LR-0, whose core layouts were settled in order to reproduce the ALFRED core conditions (*i.e.*, MOX fuel and lead coolant) – were described.


For the activity planned in VENUS-F, a focus was put on the ERANOS deterministic code (ver. 2.2), coupled with the JEFF3.1 and ENDF/B-VI.8 nuclear data libraries. The most part of the work here summarised is related to the VENUS-F experiments carried out during the EURATOM FP7 FREYA project, in which a critical layout representative of the LFR core design (called CC6 core and having a specific 3x3 assembly ALFRED island) was assembled and the usual characterisation measurements were performed. The LFR representativeness was achieved by reproducing the ALFRED spectrum above 1 keV in the experimental FA (EFA-2) embedded in such 3x3 island.

The present analysis is complementary with the studies performed in the FREYA project [8]. Some fundamental physical quantities for the core design in steady state were analysed, such as: the k_{eff} multiplication factor, the spectrum indexes, the anti-reactivity inserted by a single CR and, additionally, the main kinetic parameters. The most significant results concern:

- the C/E values for the anti-reactivity worth inserted by the CR close to the ALFRED island at different insertion height. The ERANOS worth values under-estimate the experimental ones by 6 ÷ 8%, with the the ENDF/B-VI.8 results that appear to be slightly more accurate than the JEFF3.1 ones;
- the C/E values for the spectrum indexes in the EFA-2 channel at core mid-plane. The “worst” C/E values appears for the F28/F25 and F37/F25 indexes, that deal with U^{238} and Np^{237} nuclides having a threshold fission cross-section. As suggested in [5] and referring to the F28/F25 value, this discrepancy can be reduced when considering the possibility of tiny U^{235} impurities in the U^{238} fission chamber deposit;
- the negligible effect of the neutron data library adopted (JEFF3.1 and ENDF/B-VI.8) on the main kinetic parameters: the effective delayed neutron fraction (β_{eff}) and the neutron generation lifetime (A_{eff}).

For what concerns the effective multiplication factor (in VENUS-F):


- the impact on the k_{eff} value due to small variations of some materials properties appears to be significant, as for the fuel density (with a $\Delta k_{\text{eff}} \approx 460$ pcm per 1 wt.% variation) and the U^{235} enrichment (with a $\Delta k_{\text{eff}} \approx 470$ pcm per 1 wt.% variation);
- even if VENUS-F is a zero power reactor, the fuel doppler effect was investigated by obtaining a $\Delta k_{\text{eff}} \approx -0.5$ pcm per 1 °C variation in the 20 ÷ 200 °C range;
- sensitivity and uncertainty analyses were performed (see Appendix A), also because the neutronic studies in FREYA pointed out a significant spread in the k_{eff} value due to the code (Monte Carlo or deterministic) and the library adopted [8]. Actually, these analyses indicate that a reduction of the uncertainties on nuclear data could reduce significantly such discrepancies. In fact, by summing conservatively over the contributions of every isotope, cross-section and energy group, a Δk_{eff} variation of about 2000 pcm (*i.e.*, 2%) is obtained. The ERANOS results with JEFF3.1 and

| | | | | | |
|--|---------------------------------|-------------|-----------------|-------------|-----------|
|  Ricerca Sistema Elettrico | Sigla di identificazione | Rev. | Distrib. | Pag. | di |
| | ADPFISS – LP2 – 115 | 0 | L | 19 | 32 |

ENDF/B-VI.8 data libraries show similar trends and values: as expected, in both cases the highest contributions to the k_{eff} uncertainty comes from the U isotopes, mainly from the U^{235} capture cross-section in the energy range approximately between 10 keV and 1.5 MeV. Then, also the fission cross-sections and the average number of neutrons emitted per fission of both U^{235} and U^{238} isotopes yield significant contributions in the same energy range, as well as the U^{238} inelastic cross-section.


For what concerns the activities envisaged in the LR-0 reactor, the design of the experimental test section to be installed within the core, as well as the definition of the core configuration fitting with the test section itself, were performed. To target these aimed results, a thorough analysis was performed so as to investigate the optimal configurations of test section and sustaining core permitting to attain a neutron spectrum as relevantly as possible reproducing the one proper of ALFRED. Parametric investigations were performed to anticipate, hence assess, the impact of the construction materials and measurement devices on the results of the envisaged experiments.

At the end of this preliminary simulation and design activities, the experimental test section has been realized and installed into the core of the LR-0 reactor. The tests, expected by the end of the present year, will provide the measurements requested by ENEA to perform the validation of the corresponding calculation models, already implemented with the MCNP code (ver. 6.1) to execute the simulations required to support the design of the experiments.


| | | | | | |
|--|---------------------------------|-------------|-----------------|-------------|-----------|
|  Ricerca Sistema Elettrico | Sigla di identificazione | Rev. | Distrib. | Pag. | di |
| | ADPFISS – LP2 – 115 | 0 | L | 20 | 32 |

References

- [1] Grasso, G., *et al.*, 2014. The core design of ALFRED, a demonstrator for the European lead-cooled reactors. *Nucl. Eng. and Des.*, Vol. **278**, 287-301.
- [2] OECD/NEA, 2014. Technology Roadmap Update for Generation IV Nuclear Energy Systems, www.gen-4.org.
- [3] Kochetkov, A., *et al.*, 2013. Current progress and future plans of the FREYA Project. Proc. Int. Conf. *Technology and Components of Accelerator Driven Systems (TCADS-2)*, Nantes, France, May 21-23.
- [4] <http://cvrez.cz/en/infrastructure/research-reactor-lr-0/>.
- [5] Kochetkov, A., *et al.*, 2016. Spectrum Index and Minor Actinide fission rate measurements in several fast lead critical cores in the zero power VENUS-F reactor. Proc. Int. Conf. *Unifying Theory and Experiments in the 21st Century (PHYSOR 2016)*, Sun Valley, Idaho, USA, May 1-5.
- [6] Sarotto, M., *et al.*, 2015. LFR mock-up definition. Deliverable D4.1 EURATOM FP7 “FREYA” project (Technical Report FSN-SICNUC-002, ENEA).
- [7] Kochetkov, A., *et al.*, 2015. LFR mock-up characterisation, Deliverable D4.2 EURATOM FP7 “FREYA” project.
- [8] Sarotto, M., *et al.*, 2015. LFR mock-up reactivity effects, Deliverable D4.3 EURATOM FP7 “FREYA” project (Technical Report FSN-SICNUC-003, ENEA).
- [9] Rimpault, G., *et al.*, 2002. The ERANOS code and data system for Fast Reactor neutronic analyses. Proc. Int. Conf. *New Frontiers of Nuclear Technology: reactor physics, safety and high-performance computing (PHYSOR 2002)*, Seoul, Korea, October 7-10.
- [10] Rimpault, G., 1997. Physics documentation of Eranos: the Ecco cell code. Technical Report DERSPRC-LEPh-97-001, CEA.
- [11] Ruggeri, J.M., *et al.*, 1993. TGV: a coarse mesh 3 dimensional diffusion-transport module for the CCRR/ERANOS code system. Technical Report DRNR-SPCILEPh-93-209, CEA.
- [12] Koning, A., *et al.*, 2006. The JEFF-3.1 Nuclear Data Library, NEA Data Bank. Technical Report JEFF Report 21, NEA N_6190, OECD.
- [13] <https://www-nds.iaea.org/exfor/endl.htm>
- [14] Bianchini, G., *et al.*, 2011. Guinevere project: updated deterministic model by the ERANOS French code. Technical Report UTFISSM-P9US-001, ENEA.
- [15] Salvatores, M., *et al.*, 2008. Uncertainty and target accuracy assessment for innovative systems using recent covariance data evaluations (International Evaluation Co-operation Volume 26), OECD/NEA WPEC-26 ISBN 978-92-64-99053-1, Technical Rep. No. 6410, OECD.
- [16] Goorley, J.T., *et al.*, 2013. Initial MCNP6 Release Overview - MCNP6 version 1.0. Technical Report LA-UR-13-22934, Los Alamos National Laboratories.

| | | | | | |
|--|---------------------------------|-------------|-----------------|-------------|-----------|
|  Ricerca Sistema Elettrico | Sigla di identificazione | Rev. | Distrib. | Pag. | di |
| | ADPFISS – LP2 – 115 | 0 | L | 21 | 32 |

- [17] Chadwick, M.B., *et al.*, 2006. ENDF/B-VII.0: Next Generation Evaluated Nuclear Data Library for Nuclear Science and Technology. *Nucl. Data Sheets* **107(12)**. Also in Technical Report UCRL-JRNL-225066.
- [18] Sarotto, M., 2015. The VENUS-F CC6 core: ERANOS neutronic analyses and comparison with experimental data. Presentation at EURATOM FP7 “FREYA WP3/4 meeting, Genova (I), November 12-13 (Technical Report FSN-SICNUC-004, ENEA).
- [19] Losa E. and Košťál M., 2015. Design and preparation of experiment for validation of neutronic codes. Technical Report 1157, CVŘ.
- [20] Tommasi, J., 2006. Standard perturbation theory and applications. Presentation at ERANOS users’ workshop, Cadarache (F), May 29-June 2.

| | | | | | |
|--|---------------------------------|-------------|-----------------|-------------|-----------|
|  Ricerca Sistema Elettrico | Sigla di identificazione | Rev. | Distrib. | Pag. | di |
| | ADPFISS – LP2 – 115 | 0 | L | 22 | 32 |

Appendix A - Sensitivity and uncertainty analyses on k_{eff} value

A.1. Brief summary of background theory

The approach used for this kind of analyses on the multiplication factor value (k_{eff} or easily k) includes [15]:

- a sensitivity study using the perturbation theory;
- an uncertainty assessment using covariance data.

The sensitivity study was based on the adjoint approach, that is implemented in ERANOS [20]. By definition, the sensitivity coefficients give the rate of change of a parameter (k in this case) as a function of a variation of another parameter (the cross-sections σ in this case):

$$S_k = \frac{\partial k}{\partial \sigma} \frac{\sigma}{k} \quad (\text{A.1})$$

The variation of the cross-sections causes a variation of the Boltzmann operator (here named M) that can be evaluated linearly by adopting the standard perturbation theory. In some details, by calculating the direct and adjoint fluxes in the critical system (Φ and Φ^* , respectively):

$$M\Phi = \left(A - \frac{1}{k}F \right) \Phi = 0 \quad (\text{A.2})$$

$$M^*\Phi^* = \left(A^* - \frac{1}{k}F^* \right) \Phi^* = 0 \quad (\text{A.3})$$

where A is the loss (leakage + absorption) operator and F is the fission production operator, the sensitivity coefficient (A.1) can be evaluated by adopting the standard perturbation theory with:

$$S_k = -k \frac{\langle \Phi^*, \left(A - \frac{F}{k} \right) \Phi \rangle}{\langle \Phi^*, F\Phi \rangle} \quad (\text{A.4})$$

where “ $\langle \ , \ \rangle$ ” denotes the integration over space, angle and energy. In the present analysis the diffusion approximation was utilised. Consequently:

- the scalar flux is adopted, starting from an original angular flux evaluated by the S8 symmetric discretisation [9] and cross-sections calculated at the first order (P1) of the Legendre polynomials [10];
- consequently, the integration “ $\langle \ , \ \rangle$ ” is limited over space and energy.

Nevertheless, the errors introduced by the diffusion approximation (*e.g.*, valid for large systems only) are partially compensated by the ratio of the space-energy integrals appearing both at numerator and denominator in (A.4). To be noticed that, differently from the results reported in §4.1-4.3 obtained with a 49 energy-group-structure, these evaluations were performed by adopting the standard structure at 33 energy groups (as in §4.4).

The sensitivity coefficients (A.4) permits to link the uncertainties on nuclear data with the uncertainty on the k value by adopting a dispersion or covariance matrix (B) and the relation:


$$\sigma_k^2 = S_k B S_k^t \quad (\text{A.5})$$

In other words, the sensitivity analysis (A.4) is obtained by adopting a unitary covariance matrix, that is diagonal with all the dispersion values for all the isotopes and all the cross-sections in each energy group equal to one (*i.e.*, $\sigma_k \equiv S_k$).

Otherwise, in the uncertainty analysis (A.5) the integral parameter uncertainties are calculated using the BOLNA covariance matrix (*i.e.*, B), developed through a joint effort of several laboratories (Brookhaven, Oak Ridge, Los Alamos, NRG Petten and Argonne). As specified in [15], there is a strong impact of correlation data (*i.e.*, off-diagonal elements) on the uncertainty assessment and any credible uncertainty analysis should include the best available covariance data accounting for energy correlations (as in the present study) and possibly for cross-correlations among reactions (*e.g.*, inter-relation among total, elastic and inelastic cross-sections) and even for cross-correlation among isotopes (if needed, *e.g.*, to account for normalisation issues). The BOLNA matrix adopts a 15 energy-group-structure below 20 MeV: the relationship between the structures at 33 and 15 groups is shown in Table A.1 indicating the upper energy value of each group.

Table A.1 Relationship between energy structures at 33 and 15 groups used for the sensitivity and uncertainty analysis, respectively.

| Group N. | Energy [MeV] | Group N. | Energy [MeV] |
|----------|--------------|----------|--------------|
| 1 | 1.96403E+01 | 1 | 1.96403E+01 |
| 2 | 1.00000E+01 | 2 | 6.06531E+00 |
| 3 | 6.06531E+00 | 3 | 2.23130E+00 |
| 4 | 3.67879E+00 | 4 | 1.35335E+00 |
| 5 | 2.23130E+00 | 5 | 4.97871E-01 |
| 6 | 1.35335E+00 | 6 | 1.83156E-01 |
| 7 | 8.20850E-01 | 7 | 6.73795E-02 |
| 8 | 4.97871E-01 | 8 | 2.47875E-02 |
| 9 | 3.01974E-01 | 9 | 9.11882E-03 |
| 10 | 1.83156E-01 | 10 | 2.03468E-03 |
| 11 | 1.11090E-01 | 11 | 4.53999E-04 |
| 12 | 6.73795E-02 | 12 | 2.26033E-05 |
| 13 | 4.08677E-02 | 13 | 4.00000E-06 |
| 14 | 2.47875E-02 | 14 | 5.40000E-07 |
| 15 | 1.50344E-02 | 15 | 1.00000E-07 |
| 16 | 9.11882E-03 | | |
| 17 | 5.53084E-03 | | |
| 18 | 3.35463E-03 | | |
| 19 | 2.03468E-03 | | |
| 20 | 1.23410E-03 | | |
| 21 | 7.48518E-04 | | |
| 22 | 4.53999E-04 | | |
| 23 | 3.04325E-04 | | |
| 24 | 1.48625E-04 | | |
| 25 | 9.16609E-05 | | |
| 26 | 6.79041E-05 | | |
| 27 | 4.01690E-05 | | |
| 28 | 2.26033E-05 | | |
| 29 | 1.37096E-05 | | |
| 30 | 8.31529E-06 | | |
| 31 | 4.00000E-06 | | |
| 32 | 5.40000E-07 | | |
| 33 | 1.00000E-07 | | |

| | | | | | |
|--|---------------------------------|-------------|-----------------|-------------|-----------|
|  Ricerca Sistema Elettrico | Sigla di identificazione | Rev. | Distrib. | Pag. | di |
| | ADPFISS – LP2 – 115 | 0 | L | 24 | 32 |

A.2. Results and discussion

The sensitivity and uncertainty analyses were carried out in ERANOS by adopting both the JEFF3.1 and ENDF/B-VI.8 nuclear data libraries. The nuclides considered were:

- U^{235} , U^{238} , Fe^{56} , Pb^{206} , Pb^{207} , Pb^{208} , Cr^{50} , Cr^{52} , Cr^{53} , Cr^{54} , Al^{27} and O^{16} in the sensitivity analysis at 33 energy groups;
- U^{235} , U^{238} , Fe^{56} , Pb^{206} , Pb^{207} , Pb^{208} , Cr^{52} , Al^{27} and O^{16} in the uncertainty analysis at 15 energy groups (since the other Cr isotopes are not included in the BOLNA covariance matrix, §A.1).

Figures A.1 and A.2 report the ERANOS values with JEFF3.1 and ENDF/B-VI.8 data, respectively, of the sensitivity coefficients per each energy group and per each cross-section, summed over the isotopes considered. Figures A.3 and A.4 report the ERANOS values with JEFF3.1 and ENDF/B-VI.8 data, respectively, of the sensitivity coefficients per each isotope considered and per each cross-section, summed over the 33 energy groups. It can be noticed that the JEFF3.1 and ENDF/B-VI.8 results show similar trends and values in both cases. The highest values appear for the sensitivity coefficients related to:

- the fission cross-sections (impacting also on the production term “ $\nu \cdot \Sigma_f$ ”) and, mainly, the average number of neutrons emitted per fission ($NU \equiv \nu$) in the energy range approximatively between the 4th and 16th group, that corresponds to the interval between 10 keV and 3 MeV. As shown in Figures A.1 and A.2, also the capture cross-sections yield a significant (negative) contribute for both libraries;
- the capture and fission cross-sections and the average number of neutrons emitted per fission (NU) by the U^{235} and U^{238} isotopes, as shown in Figures A.3 and A.4.

It can be further noticed that almost all the sensitivity coefficients are positive, by the exception the capture ones (for each energy value) and the n,xn reactions at higher energies.

For what concerns the uncertainty analysis:

- Tables A.2 and A.3 report the ERANOS values with JEFF3.1 and ENDF/B-VI.8 data, respectively, of the uncertainty on the k_{eff} values summed over the 15 energy groups per each isotope considered and per each cross-section, while Figures A.5 and A.6 show them in a graphical form. The JEFF3.1 and ENDF/B-VI.8 results are similar and the highest contribution is due to the U^{235} capture term. Significant contributions appear also for NU and fission cross-section of U^{235} , together with NU, capture and inelastic cross-sections of U^{238} ;
- Tables A.4 and A.5 report the ERANOS values with JEFF3.1 and ENDF/B-VI.8 data, respectively, of the uncertainty values on the k_{eff} values summed over the isotopes considered per each energy group and per each cross-section, while Figures A.7 and A.8 show them in a graphical form. The JEFF3.1 and ENDF/B-VI.8 results are similar and the highest contribution is due to the U^{235} capture in the energy range approximatively between the 4th and 9th group, that corresponds to the interval between 10 keV and 1.5 MeV;
- Tables A.6 and A.7 report the ERANOS values with JEFF3.1 and ENDF/B-VI.8 data, respectively, of the uncertainty values on the k_{eff} values summed over the cross-sections per each isotope considered and per each energy group, while Figures A.9 and A.10 show them in a graphical form. The JEFF3.1 and ENDF/B-VI.8 results are

similar and the highest contribution is due to the U^{235} isotope in the energy range approximately between 10 keV and 1.5 MeV. A significant contribution is also due to the U^{238} isotope at higher energies, probably for the threshold behaviour of its fission cross-section.

As a whole, each term (*i.e.*, cross-section and NU values) yields a significant uncertainty on the k_{eff} value of about 2% with both libraries, that corresponds to a Δk_{eff} of 2000 pcm. To be noticed that, being an uncertainty analysis, the total of the row and column values in Tables A.2-A.7 are obtained by the square root of the sum of the square of each term.

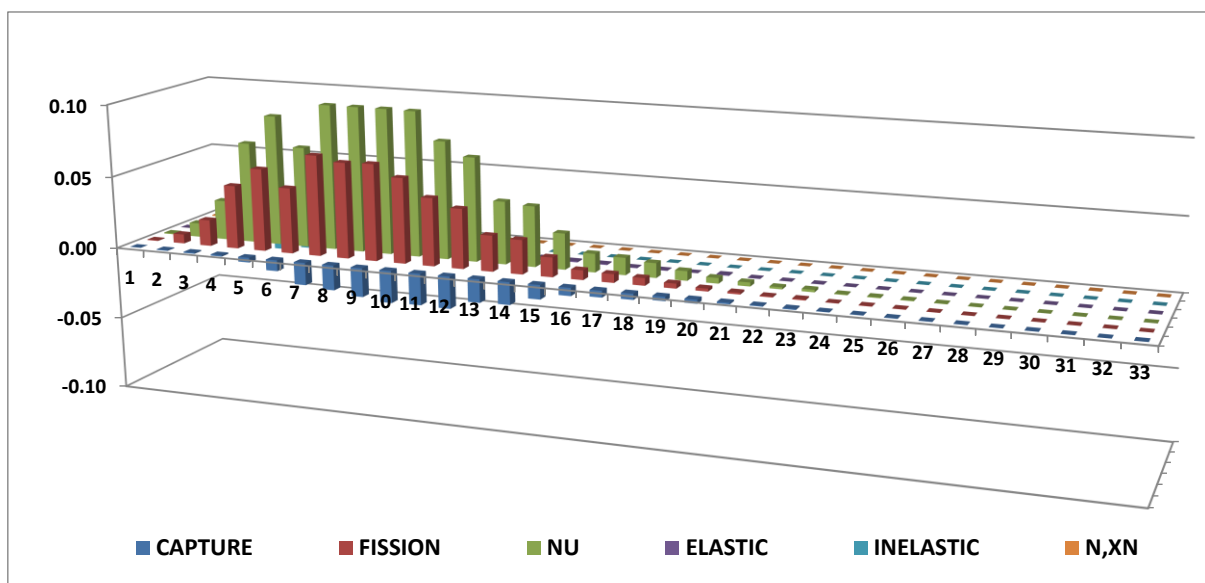


Figure A.1 ERANOS-JEFF3.1 values of the sensitivity coefficients summed over the isotopes per each energy group and per each cross-section.

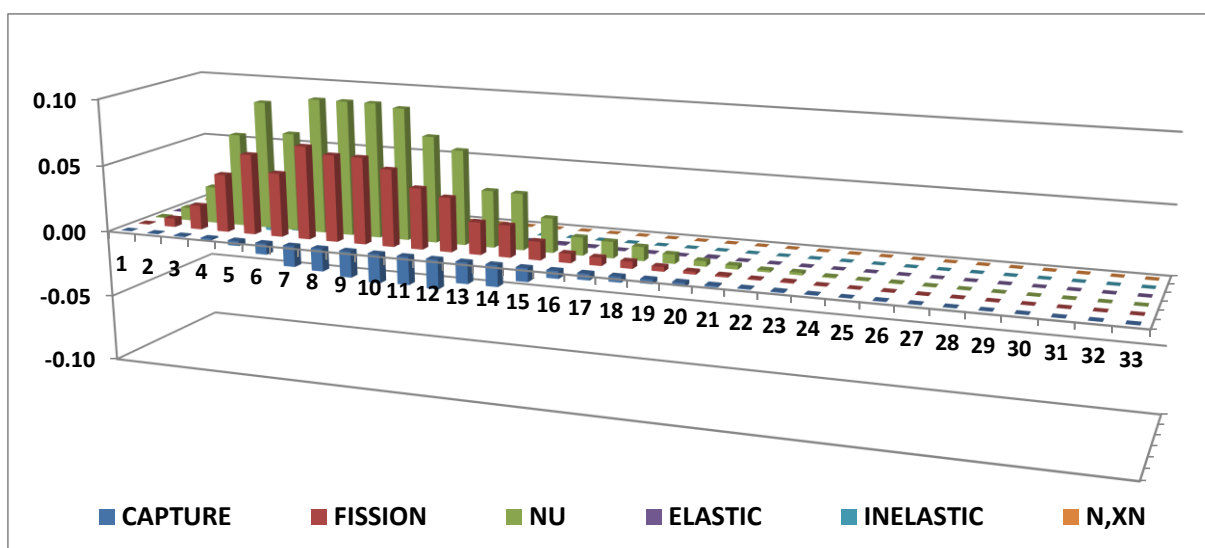


Figure A.2 ERANOS-ENDF/B-VI.8 values of the sensitivity coefficients summed over the isotopes per each energy group and per each cross-section.

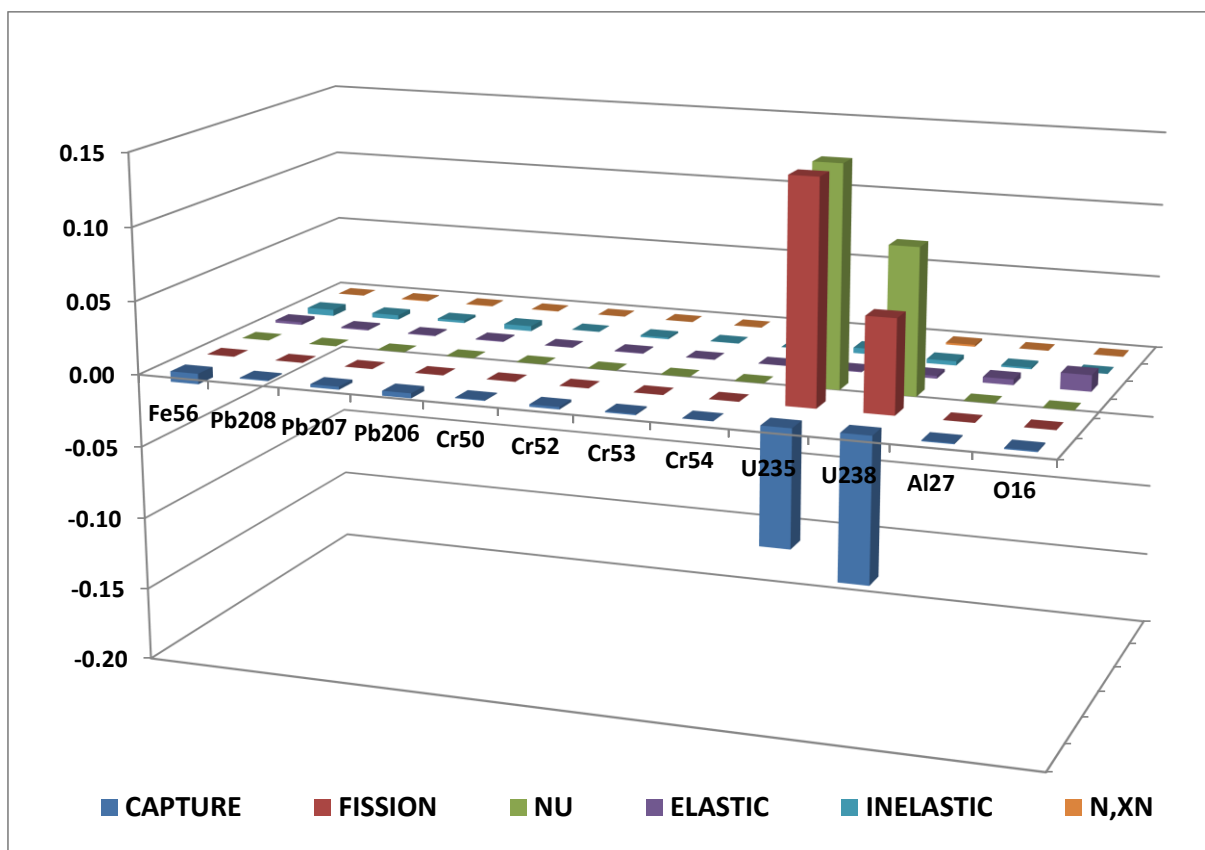


Figure A.3 Eranos-JEFF3.1 values of the sensitivity coefficients summed over the 33 energy groups per each isotope and per each cross-section.

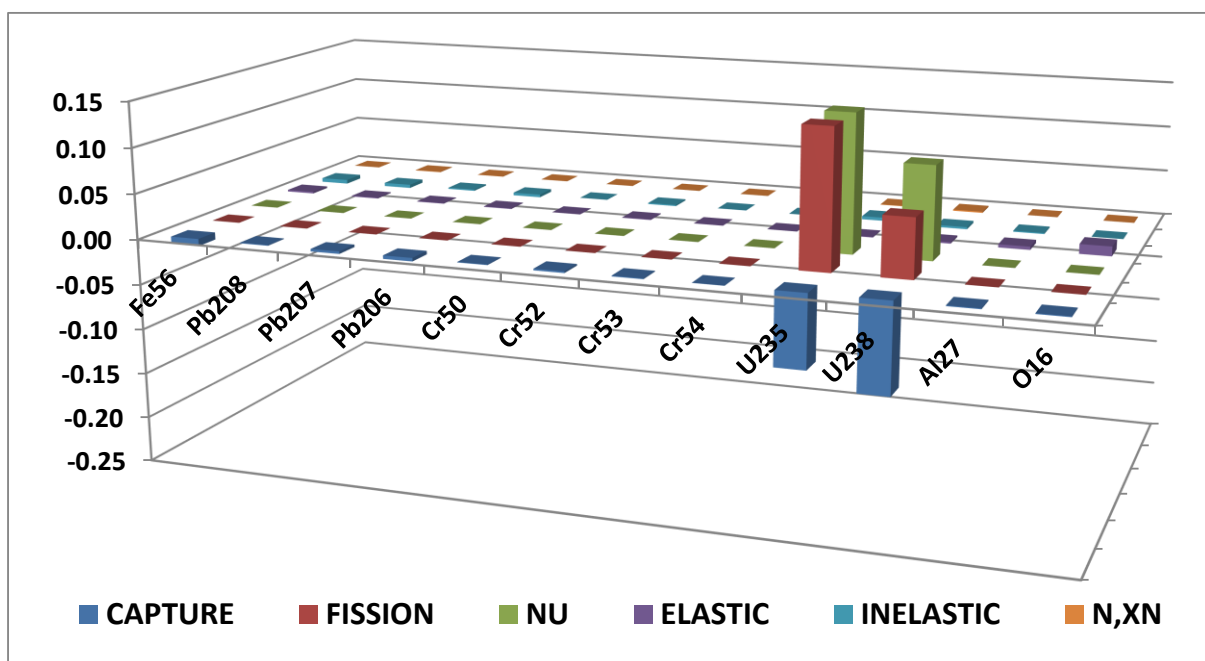


Figure A.4 Eranos-ENDF/B-VI.8 values of the sensitivity coefficients summed over the 33 energy groups per each isotope and per each cross-section.

Table A.2 ERANOS-JEFF3.1 results of the uncertainty on the k_{eff} values summed over the 15 energy groups per each isotope considered and per each cross-section.

| Isotope | CAPTURE | FISSION | NU | ELASTIC | INELASTIC | N, XN | TOTAL |
|--------------|-----------------|-----------------|-----------------|-----------------|-----------------|-----------------|-----------------|
| Fe56 | 3.40E-04 | 0.00E+00 | 0.00E+00 | 5.69E-05 | 3.73E-04 | 7.83E-07 | 5.08E-04 |
| Pb208 | 1.41E-04 | 0.00E+00 | 0.00E+00 | 5.13E-05 | 2.27E-04 | 2.51E-05 | 2.73E-04 |
| Pb207 | 3.16E-04 | 0.00E+00 | 0.00E+00 | 2.05E-05 | 1.67E-04 | 1.61E-05 | 3.58E-04 |
| Pb206 | 5.02E-04 | 0.00E+00 | 0.00E+00 | 2.54E-05 | 2.56E-04 | 6.97E-06 | 5.64E-04 |
| Cr52 | 5.51E-05 | 0.00E+00 | 0.00E+00 | 3.74E-05 | 3.03E-05 | 1.61E-07 | 7.31E-05 |
| U235 | 2.07E-02 | 2.31E-03 | 5.37E-03 | 4.69E-04 | 5.94E-04 | 8.66E-05 | 2.15E-02 |
| U238 | 1.70E-03 | 3.36E-04 | 1.11E-03 | 1.03E-04 | 1.93E-03 | 7.17E-05 | 2.82E-03 |
| Al27 | 7.72E-05 | 0.00E+00 | 0.00E+00 | 6.06E-05 | 2.02E-04 | 2.72E-08 | 2.25E-04 |
| O16 | 6.10E-04 | 0.00E+00 | 0.00E+00 | 2.05E-04 | 6.77E-05 | 3.52E-10 | 6.47E-04 |
| TOTAL | 2.08E-02 | 2.33E-03 | 5.49E-03 | 5.13E-04 | 2.10E-03 | 1.17E-04 | 0.0217 |

Table A.3 ERANOS- ENDF/B-VI.8 results of the uncertainty on the k_{eff} values summed over the 15 energy groups per each isotope considered and per each cross-section.

| Isotope | CAPTURE | FISSION | NU | ELASTIC | INELASTIC | N, XN | TOTAL |
|--------------|-----------------|-----------------|-----------------|-----------------|-----------------|-----------------|-----------------|
| Fe56 | 3.63E-04 | 0.00E+00 | 0.00E+00 | 5.79E-05 | 3.98E-04 | 7.22E-07 | 5.42E-04 |
| Pb208 | 1.44E-04 | 0.00E+00 | 0.00E+00 | 5.13E-05 | 2.42E-04 | 2.20E-05 | 2.87E-04 |
| Pb207 | 4.26E-04 | 0.00E+00 | 0.00E+00 | 2.19E-05 | 1.58E-04 | 1.25E-05 | 4.55E-04 |
| Pb206 | 5.74E-04 | 0.00E+00 | 0.00E+00 | 2.87E-05 | 2.30E-04 | 5.98E-06 | 6.19E-04 |
| Cr52 | 5.48E-05 | 0.00E+00 | 0.00E+00 | 4.08E-05 | 3.28E-05 | 1.50E-07 | 7.58E-05 |
| U235 | 2.05E-02 | 2.30E-03 | 5.35E-03 | 4.55E-04 | 5.70E-04 | 8.75E-05 | 2.13E-02 |
| U238 | 1.73E-03 | 3.40E-04 | 1.14E-03 | 1.48E-04 | 1.89E-03 | 7.13E-05 | 2.82E-03 |
| Al27 | 7.96E-05 | 0.00E+00 | 0.00E+00 | 5.60E-05 | 2.01E-04 | 2.48E-08 | 2.23E-04 |
| O16 | 6.12E-04 | 0.00E+00 | 0.00E+00 | 2.28E-04 | 6.85E-05 | 3.17E-10 | 6.57E-04 |
| TOTAL | 2.06E-02 | 2.32E-03 | 5.47E-03 | 4.99E-04 | 2.06E-03 | 1.16E-04 | 0.0215 |

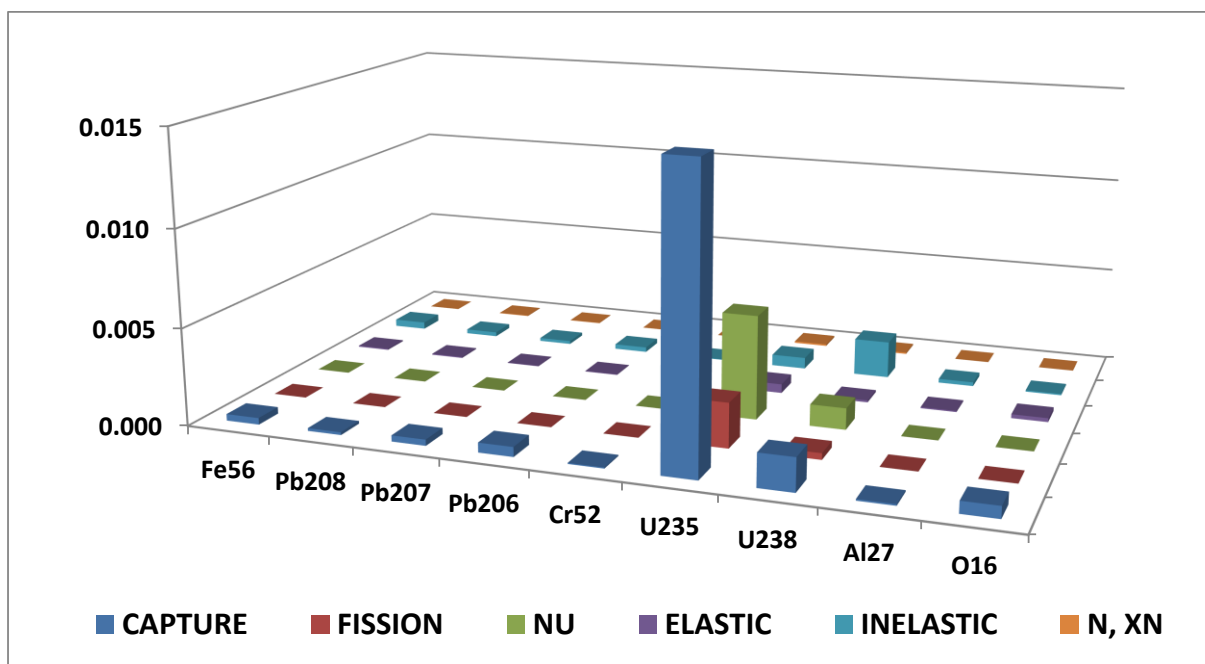


Figure A.5 ERANOS-JEFF3.1 results of the uncertainty on the k_{eff} values summed over the 15 energy groups per each isotope considered and per each cross-section.

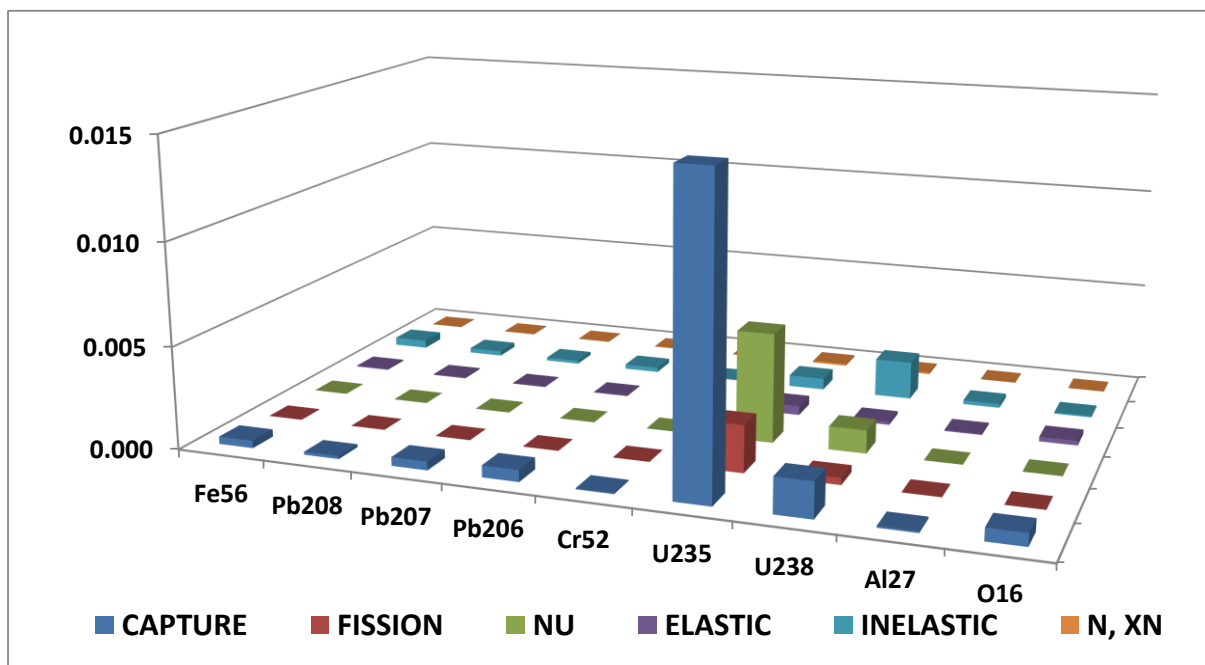


Figure A.6 ERANOS-ENDF/B-VI.8 results of the uncertainty on the k_{eff} values summed over the 15 energy groups per each isotope considered and per each cross-section.

Table A.4 ERANOS-JEFF3.1 results of the uncertainty on the k_{eff} values summed over the isotopes considered per each energy group and per each cross-section.

| Group N. | CAPTURE | FISSION | NU | ELASTIC | INELASTIC | N, XN | TOTAL |
|--------------|-----------------|-----------------|-----------------|-----------------|-----------------|-----------------|-----------------|
| 1 | 3.00E-04 | 1.59E-04 | 4.02E-04 | 1.01E-04 | 6.15E-04 | 1.17E-04 | 8.24E-04 |
| 2 | 1.74E-04 | 5.24E-04 | 1.36E-03 | 1.02E-04 | 1.73E-03 | 2.81E-06 | 2.27E-03 |
| 3 | 1.22E-03 | 5.53E-04 | 1.35E-03 | 8.78E-05 | 1.39E-03 | 0.00E+00 | 2.36E-03 |
| 4 | 4.08E-03 | 9.99E-04 | 2.19E-03 | 2.74E-04 | 1.08E-03 | 0.00E+00 | 4.62E-03 |
| 5 | 8.36E-03 | 1.14E-03 | 2.65E-03 | 3.33E-04 | 4.59E-04 | 0.00E+00 | 8.86E-03 |
| 6 | 1.12E-02 | 1.02E-03 | 2.51E-03 | 1.46E-04 | 2.65E-04 | 0.00E+00 | 1.15E-02 |
| 7 | 1.02E-02 | 7.69E-04 | 1.99E-03 | 1.33E-04 | 1.41E-04 | 0.00E+00 | 1.04E-02 |
| 8 | 8.47E-03 | 5.64E-04 | 1.52E-03 | 1.46E-04 | 4.35E-06 | 0.00E+00 | 8.62E-03 |
| 9 | 6.48E-03 | 7.63E-04 | 1.09E-03 | 6.55E-05 | 3.42E-09 | 0.00E+00 | 6.62E-03 |
| 10 | 2.40E-04 | 8.96E-05 | 6.70E-04 | 7.70E-06 | 0.00E+00 | 0.00E+00 | 7.06E-04 |
| 11 | 7.47E-05 | 2.11E-05 | 4.05E-04 | 1.30E-05 | 0.00E+00 | 0.00E+00 | 4.12E-04 |
| 12 | 3.03E-05 | 5.04E-06 | 9.88E-05 | 3.64E-06 | 0.00E+00 | 0.00E+00 | 1.03E-04 |
| 13 | 2.13E-05 | 9.77E-07 | 5.71E-05 | 6.99E-07 | 0.00E+00 | 0.00E+00 | 6.09E-05 |
| 14 | 1.21E-05 | 7.25E-07 | 2.19E-05 | 1.53E-07 | 0.00E+00 | 0.00E+00 | 2.51E-05 |
| 15 | 3.04E-06 | 2.03E-07 | 5.89E-06 | 0.00E+00 | 0.00E+00 | 0.00E+00 | 6.63E-06 |
| TOTAL | 2.08E-02 | 2.33E-03 | 5.49E-03 | 5.13E-04 | 2.10E-03 | 1.17E-04 | 0.0217 |

Table A.5 ERANOS-ENDF/B-VI.8 results of the uncertainty on the k_{eff} values summed over the isotopes considered per each energy group and per each cross-section.

| Group N. | CAPTURE | FISSION | NU | ELASTIC | INELASTIC | N, XN | TOTAL |
|--------------|-----------------|-----------------|-----------------|-----------------|-----------------|-----------------|-----------------|
| 1 | 3.05E-04 | 1.59E-04 | 4.03E-04 | 1.11E-04 | 5.66E-04 | 1.16E-04 | 7.92E-04 |
| 2 | 1.99E-04 | 5.26E-04 | 1.37E-03 | 1.33E-04 | 1.62E-03 | 2.84E-06 | 2.20E-03 |
| 3 | 1.26E-03 | 5.66E-04 | 1.40E-03 | 1.0185E-04 | 1.44E-03 | 0.00E+00 | 2.43E-03 |
| 4 | 4.14E-03 | 1.01E-03 | 2.22E-03 | 2.63E-04 | 1.03E-03 | 0.00E+00 | 4.70E-03 |
| 5 | 8.25E-03 | 1.12E-03 | 2.62E-03 | 3.16E-04 | 4.49E-04 | 0.00E+00 | 8.75E-03 |
| 6 | 1.10E-02 | 1.00E-03 | 2.47E-03 | 1.37E-04 | 2.61E-04 | 0.00E+00 | 1.13E-02 |
| 7 | 1.00E-02 | 7.56E-04 | 1.97E-03 | 1.27E-04 | 1.46E-04 | 0.00E+00 | 1.03E-02 |
| 8 | 8.50E-03 | 5.66E-04 | 1.52E-03 | 1.49E-04 | 4.38E-06 | 0.00E+00 | 8.65E-03 |
| 9 | 6.56E-03 | 7.81E-04 | 1.11E-03 | 6.54E-05 | 3.31E-09 | 0.00E+00 | 6.70E-03 |
| 10 | 2.55E-04 | 9.29E-05 | 6.83E-04 | 1.37E-05 | 0.00E+00 | 0.00E+00 | 7.23E-04 |
| 11 | 8.13E-05 | 2.22E-05 | 4.14E-04 | 1.28E-05 | 0.00E+00 | 0.00E+00 | 4.22E-04 |
| 12 | 3.22E-05 | 5.39E-06 | 1.03E-04 | 2.65E-06 | 0.00E+00 | 0.00E+00 | 1.08E-04 |
| 13 | 2.44E-05 | 1.24E-06 | 5.67E-05 | 9.77E-07 | 0.00E+00 | 0.00E+00 | 6.17E-05 |
| 14 | 9.11E-06 | 5.30E-07 | 1.53E-05 | 3.34E-07 | 0.00E+00 | 0.00E+00 | 1.78E-05 |
| 15 | 2.09E-06 | 1.23E-07 | 3.28E-06 | 0.00E+00 | 0.00E+00 | 0.00E+00 | 3.89E-06 |
| TOTAL | 2.06E-02 | 2.32E-03 | 5.47E-03 | 4.99E-04 | 2.06E-03 | 1.16E-04 | 0.0215 |

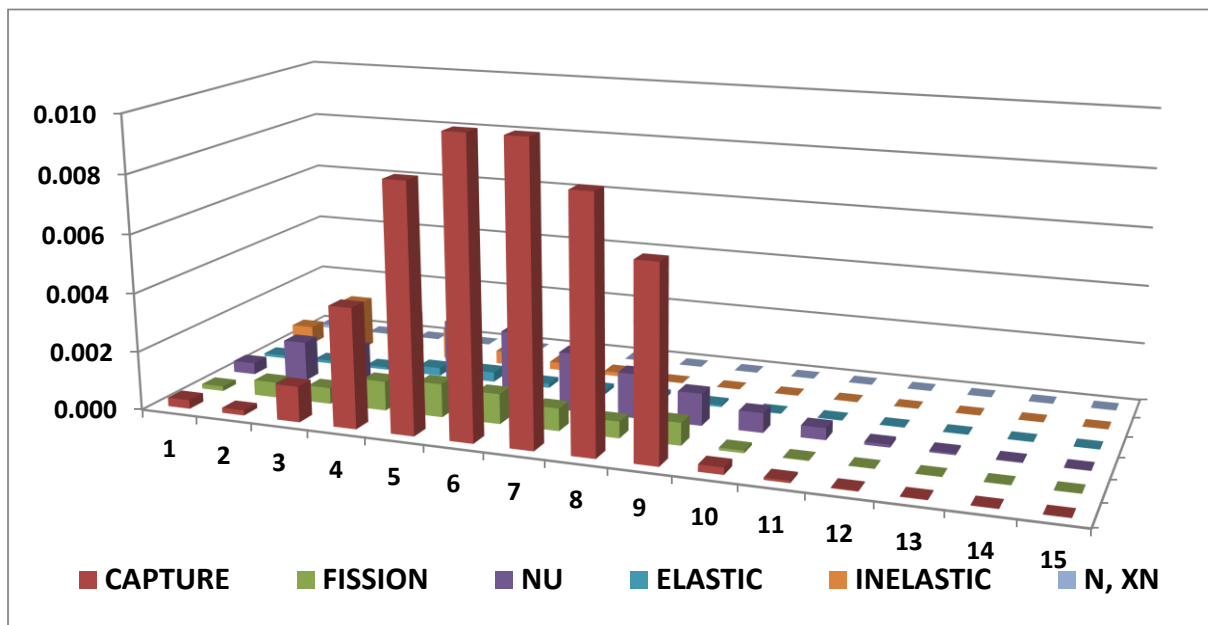


Figure A.7 Eranos-JEFF3.1 results of the uncertainty on the k_{eff} values summed over the isotopes considered per each energy group and per each cross-section.

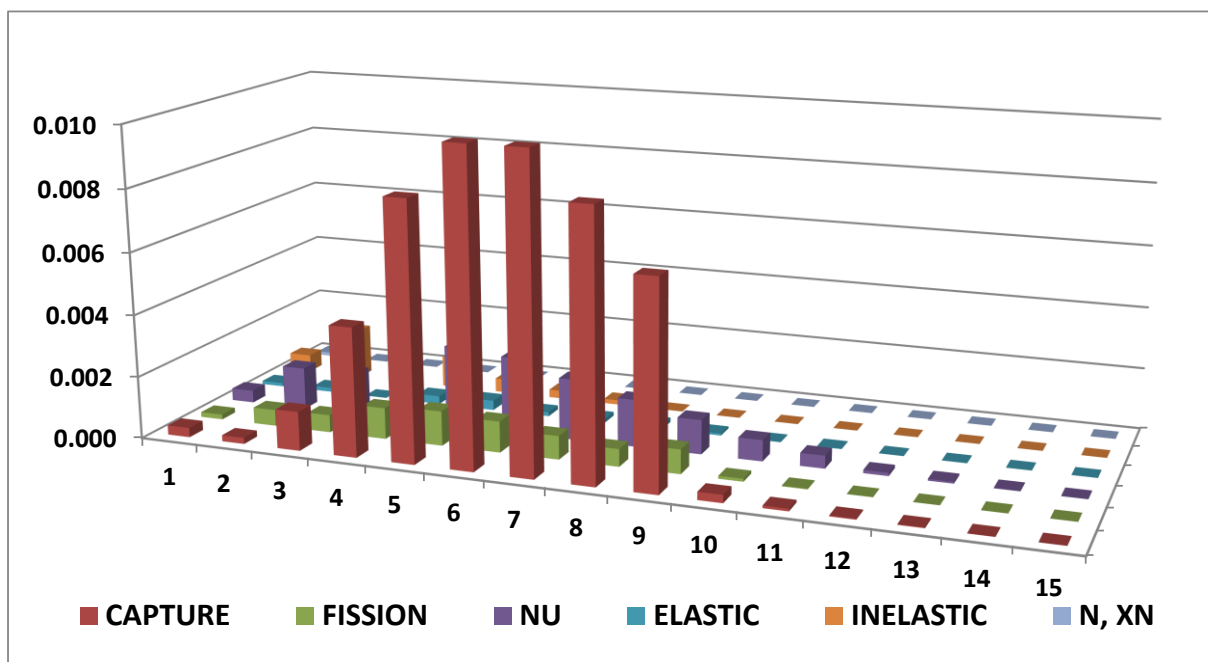


Figure A.8 Eranos-ENDF/B-VI.8 results of the uncertainty on the k_{eff} values summed over the isotopes considered per each energy group and per each cross-section.

Table A.6 ERANOS-JEFF3.1 results of the uncertainty on the k_{eff} values summed over the cross-sections per each isotope considered and per each energy group.

| Group N. | Fe56 | Pb208 | Pb207 | Pb206 | Cr52 | U235 | U238 | Al27 | O16 | TOTAL |
|--------------|-----------------|-----------------|-----------------|-----------------|-----------------|-----------------|-----------------|-----------------|-----------------|-----------------|
| 1 | 5.48E-05 | 2.05E-04 | 9.39E-05 | 1.02E-04 | 2.33E-05 | 3.78E-04 | 6.04E-04 | 6.97E-05 | 3.19E-04 | 8.24E-04 |
| 2 | 1.20E-04 | 1.05E-04 | 7.72E-05 | 1.74E-04 | 2.50E-05 | 1.08E-03 | 1.90E-03 | 1.67E-04 | 5.49E-04 | 2.27E-03 |
| 3 | 5.10E-04 | 6.12E-06 | 1.34E-04 | 1.94E-04 | 1.54E-05 | 1.72E-03 | 1.49E-03 | 1.43E-04 | 1.68E-04 | 2.36E-03 |
| 4 | 2.93E-04 | 8.95E-05 | 8.36E-05 | 1.91E-04 | 2.10E-05 | 4.73E-03 | 1.00E-03 | 7.71E-05 | 5.66E-05 | 4.62E-03 |
| 5 | 6.42E-05 | 7.63E-05 | 1.68E-04 | 2.51E-04 | 3.30E-05 | 8.84E-03 | 5.02E-04 | 5.03E-05 | 6.29E-05 | 8.86E-03 |
| 6 | 1.85E-04 | 8.57E-05 | 1.47E-04 | 2.47E-04 | 4.29E-05 | 1.15E-02 | 5.91E-04 | 2.18E-05 | 3.48E-05 | 1.15E-02 |
| 7 | 1.68E-04 | 2.02E-05 | 1.37E-04 | 2.08E-04 | 1.54E-05 | 1.04E-02 | 5.52E-04 | 1.02E-05 | 3.78E-05 | 1.04E-02 |
| 8 | 2.79E-05 | 3.14E-06 | 9.37E-05 | 1.60E-04 | 1.42E-05 | 8.52E-03 | 1.34E-03 | 9.89E-06 | 4.36E-05 | 8.62E-03 |
| 9 | 1.17E-05 | 3.05E-06 | 9.83E-05 | 1.04E-04 | 2.33E-06 | 6.61E-03 | 2.40E-04 | 4.22E-06 | 1.51E-05 | 6.62E-03 |
| 10 | 1.48E-04 | 2.04E-06 | 2.94E-05 | 9.80E-06 | 1.19E-05 | 6.84E-04 | 8.34E-05 | 2.08E-06 | 1.51E-05 | 7.06E-04 |
| 11 | 6.19E-05 | 2.62E-06 | 2.11E-05 | 6.81E-06 | 2.25E-06 | 4.06E-04 | 3.02E-05 | 8.62E-07 | 7.07E-06 | 4.12E-04 |
| 12 | 2.98E-05 | 0.00E+00 | 0.00E+00 | 0.00E+00 | 1.01E-06 | 9.90E-05 | 4.67E-06 | 3.83E-07 | 2.82E-06 | 1.03E-04 |
| 13 | 2.11E-05 | 0.00E+00 | 0.00E+00 | 0.00E+00 | 6.76E-07 | 5.71E-05 | 1.69E-06 | 4.17E-08 | 7.86E-07 | 6.09E-05 |
| 14 | 1.21E-05 | 0.00E+00 | 0.00E+00 | 0.00E+00 | 4.28E-07 | 2.20E-05 | 6.40E-07 | 3.72E-08 | 3.42E-07 | 2.51E-05 |
| 15 | 3.03E-06 | 0.00E+00 | 0.00E+00 | 0.00E+00 | 1.11E-07 | 5.89E-06 | 1.43E-07 | 1.89E-08 | 8.64E-10 | 6.63E-06 |
| TOTAL | 5.08E-04 | 2.73E-04 | 3.58E-04 | 5.64E-04 | 7.31E-05 | 2.15E-02 | 2.82E-03 | 2.25E-04 | 6.47E-04 | 0.0217 |

Table A.7 ERANOS-ENDF/B-VI.8 results of the uncertainty on the k_{eff} values summed over the cross-sections per each isotope considered and per each energy group.

| Group N. | Fe56 | Pb208 | Pb207 | Pb206 | Cr52 | U235 | U238 | Al27 | O16 | TOTAL |
|--------------|-----------------|-----------------|-----------------|-----------------|-----------------|-----------------|-----------------|-----------------|-----------------|-----------------|
| 1 | 6.29E-05 | 2.00E-04 | 8.70E-05 | 9.99E-05 | 2.51E-05 | 3.79E-04 | 5.58E-04 | 7.06E-05 | 3.25E-04 | 7.92E-04 |
| 2 | 1.29E-04 | 0.000143 | 9.35E-05 | 1.67E-04 | 2.64E-05 | 1.09E-03 | 1.81E-03 | 1.66E-04 | 5.55E-04 | 2.20E-03 |
| 3 | 5.58E-04 | 1.05E-05 | 1.39E-04 | 2.00E-04 | 1.37E-05 | 1.76E-03 | 1.54E-03 | 1.43E-04 | 1.87E-04 | 2.43E-03 |
| 4 | 3.25E-04 | 9.26E-05 | 2.25E-04 | 2.49E-04 | 2.38E-05 | 4.79E-03 | 9.40E-04 | 7.83E-05 | 6.72E-05 | 4.70E-03 |
| 5 | 6.61E-05 | 7.55E-05 | 2.00E-04 | 2.74E-04 | 3.50E-05 | 8.72E-03 | 5.03E-04 | 4.56E-05 | 7.93E-05 | 8.75E-03 |
| 6 | 1.90E-04 | 8.58E-05 | 1.70E-04 | 2.69E-04 | 4.27E-05 | 1.13E-02 | 5.76E-04 | 2.02E-05 | 4.07E-05 | 1.13E-02 |
| 7 | 1.66E-04 | 2.02E-05 | 1.56E-04 | 2.25E-04 | 1.62E-05 | 1.02E-02 | 5.48E-04 | 1.35E-05 | 4.22E-05 | 1.03E-02 |
| 8 | 2.93E-05 | 2.89E-06 | 1.10E-04 | 1.76E-04 | 1.50E-05 | 8.54E-03 | 1.39E-03 | 1.28E-05 | 5.12E-05 | 8.65E-03 |
| 9 | 1.35E-05 | 3.46E-06 | 1.16E-04 | 1.15E-04 | 3.75E-06 | 6.69E-03 | 2.48E-04 | 5.00E-06 | 1.77E-05 | 6.70E-03 |
| 10 | 1.60E-04 | 7.66E-07 | 3.46E-05 | 9.18E-06 | 1.25E-05 | 6.99E-04 | 8.73E-05 | 2.03E-06 | 1.70E-05 | 7.23E-04 |
| 11 | 6.71E-05 | 1.29E-06 | 2.53E-05 | 8.26E-06 | 3.12E-06 | 4.15E-04 | 3.28E-05 | 7.79E-07 | 8.18E-06 | 4.22E-04 |
| 12 | 3.16E-05 | 0.00E+00 | 0.00E+00 | 0.00E+00 | 8.62E-07 | 1.03E-04 | 5.10E-06 | 2.44E-07 | 1.75E-06 | 1.08E-04 |
| 13 | 2.42E-05 | 0.00E+00 | 0.00E+00 | 0.00E+00 | 8.45E-07 | 5.67E-05 | 2.67E-06 | 1.72E-07 | 9.28E-07 | 6.17E-05 |
| 14 | 9.08E-06 | 0.00E+00 | 0.00E+00 | 0.00E+00 | 3.15E-07 | 1.53E-05 | 4.62E-07 | 5.98E-08 | 3.61E-07 | 1.78E-05 |
| 15 | 2.08E-06 | 0.00E+00 | 0.00E+00 | 0.00E+00 | 7.41E-08 | 3.28E-06 | 8.02E-08 | 2.29E-08 | 7.32E-10 | 3.89E-06 |
| TOTAL | 5.42E-04 | 2.87E-04 | 4.55E-04 | 6.19E-04 | 7.58E-05 | 2.13E-02 | 2.82E-03 | 2.23E-04 | 6.57E-04 | 0.0215 |

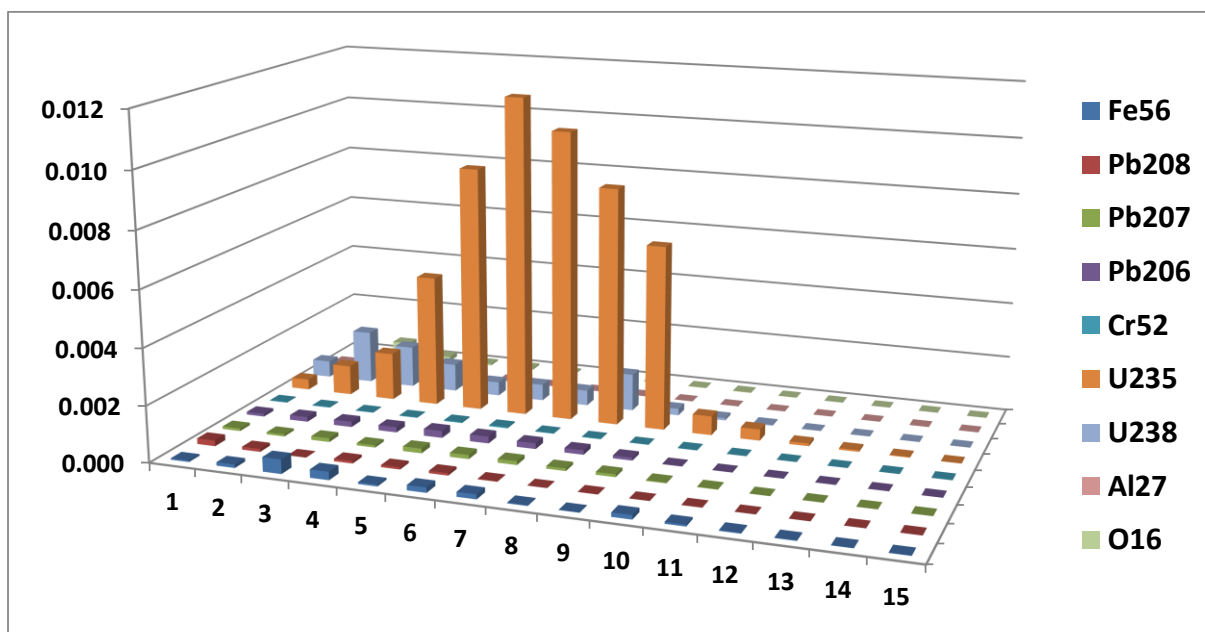


Figure A.9 ERANOS-JEFF3.1 results of the uncertainty on the k_{eff} values summed over the cross-sections per each isotope considered and per each energy group.

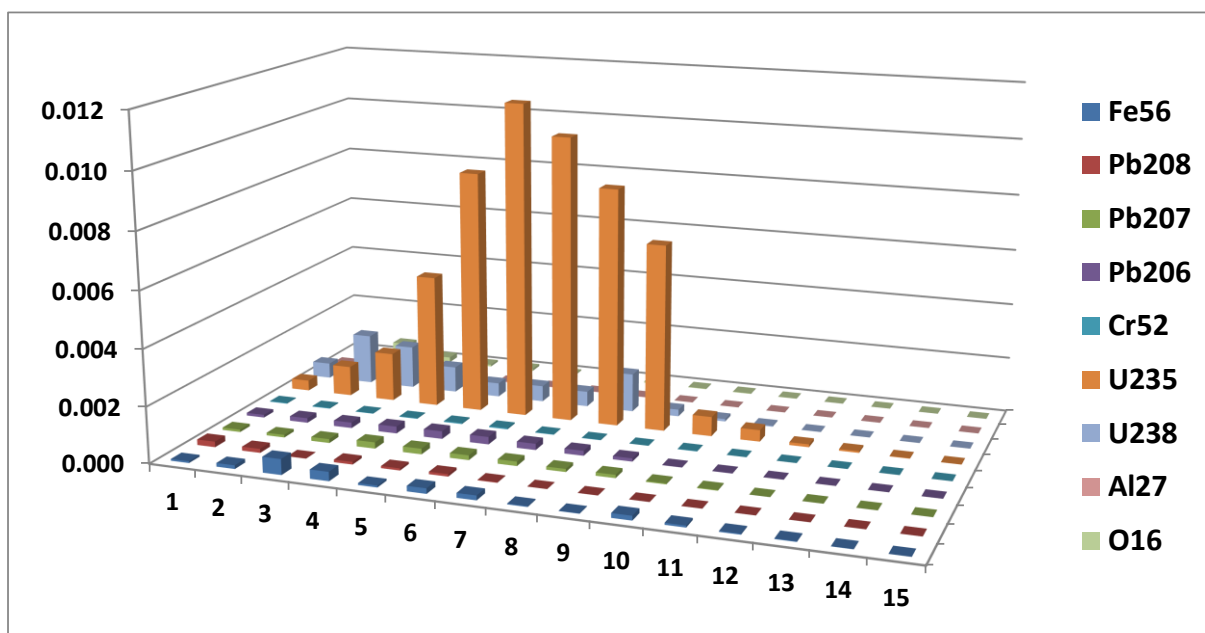


Figure A.10 ERANOS-ENDF/B-VI.8 results of the uncertainty on the k_{eff} values summed over the cross-sections per each isotope considered and per each energy group.